Journal of Marine Research, 41, 65-112, 1983

Tidally generated high-frequency internal wave packets and their effects on plankton in Massachusetts Bay

by Loren R. Haury[1], Peter H. Wiebe[2], Marshall H. Orr[3] and Melbourne G. Briscoe[2]

ABSTRACT

Tidally generated internal wave packets occur twice a day during late summer in Massachusetts Bay, U.S.A. The packets are formed at Stellwagen Bank and propagate into the Bay at about 60 cm sec^{-1}; they dissipate in shallow water at the western side of the Bay. The dominant waves in packets have lengths of about 300 m, periods of between 8 and 10 min, and amplitudes of up to 30 m. Overturning of the waves has been observed acoustically over Stellwagen Bank, in the deep (80 m) waters in the center of the Bay, and during dissipation in shallow water. The effects of the internal waves on the distribution of plankton were investigated in August 1977 using an instrument package (Longhurst-Hardy Plankton Recorder, *in situ* fluorometer, CTD) towed either at a constant depth or following an isotherm through wave packets. Phytoplankton and zooplankton appear to be carried passively up and down by the internal waves; the data were insufficient to resolve any active response by zooplankton to vertical displacements by the waves. Vertical distributions of the plankton were altered by overturning of waves and subsequent mixing. Patterns of horizontal distributions of plankton determined by constant-depth tows were dominated by the effects of internal wave vertical displacements. Isotherm-following tows removed much of the variability due to wave displacement, but problems of following rapidly moving isotherms introduced considerable smaller-scale variability. Changes in zooplankton abundance on tow length scales (600-1200 m) were not correlated with temperature, salinity, or density; some significant correlations with chlorophyll fluorescence occurred when internal wave activity was present. Twice a day for several hours or more, phytoplankton were vertically displaced by as much as 30 m, with a period of about 10 min. The light level plant cells experienced varied from 0.1 to 26% of the ambient surface illumination. This rapid change in light should alter fluorescence yields of plant cells and affect continuous *in situ* measurements of chlorophyll fluorescence. The timing of internal wave packets varies with the semidiurnal tidal cycle and therefore interacts with the day-night cycle to significantly alter the light regime experienced by plant cells over a two-week period. This could affect the primary productivity of the Bay in the area affected by internal wave packets. The sporadic occurrence of internal wave overturning and mixing events in the deep waters of the Bay could enhance primary production by increasing nutrient input to the mixed layer. This effect should be greatly enhanced in the shallow waters where the internal waves

1. Scripps Institution of Oceanography, La Jolla, California, 92093, U.S.A.
2. Woods Hole Oceanographic Institution, Woods Hole, Massachusetts, 02543, U.S.A.
3. Gulf Research and Development Company, P.O. Box 2038, Pittsburgh, Pennsylvania, 15230, U.S.A.

dissipate. Comparison of acoustic and plankton recorder data showed that much of the intense acoustic backscattering seen in high-amplitude (10-20 m) internal waves is due to physical structure and processes, and not to the presence of zooplankton.

1. Introduction

Internal waves are a ubiquitous feature of the world's oceans. Occurring with periods from tidal cycles to a few minutes, they have been invoked as significant contributors to plankton patchiness (Kamykowski, 1972; Wyatt, 1975; Haury *et al.*, 1978), to temporal and spatial variability in primary production (*e.g.*, Kamykowski, 1974, 1979) and as a source of bias and lack of precision in estimates of abundance due to interactions with sampling gear and strategies (Haury, 1976; Haury *et al.*, 1978; Angel, 1976; Denman, 1976; Kelley, 1975, 1976).

Internal waves occur in many forms; one of these is the tidally generated internal wave packet. Such packets appear to be a common phenomenon along the east coast of the United States (Sawyer and Apel, 1976) and other sites where the right combination of bathymetry, tides, and stratification occurs (Gregg and Briscoe, 1979; Maxworthy, 1979). These tidally driven internal wave packets can provide a deterministic event within which the effects on plankton of internal waves can be studied. It might be preferable to study these effects in a random, stochastic fashion in an open-ocean situation so as to provide a more general case, but this complicates both the internal wave and plankton measurements. Here, we look at the specific features of the interactions in a nearshore environment and point out in our conclusions to what extent we think these features are generalizable.

Massachusetts Bay, U.S.A., is an ideal location to observe the effects of internal wave packets on planktonic systems. In the late summer, tidally generated internal wave packets have been observed to occur twice a day (Halpern, 1971), propagating into the Bay from Stellwagen Bank (Fig. 1). Unlike tides and bathymetry, stratification varies seasonally and packets would not be expected to occur in winter. There are no year-around observations at the site to verify this. The waves are (1) easily observed visually, acoustically, and with sensors (*e.g.*, temperature, salinity, velocity) that sample sufficiently rapidly, (2) predictable in time and space, and (3) have simple, relatively uniform characteristics (speed, direction, wavelength, period).

Haury *et al.* (1979) presented preliminary results of an interdisciplinary study (27 Aug.-2 Sept. 1977) of the internal waves in Massachusetts Bay designed to investigate their generation and propagation, to describe the biological effects on the plankton, and to evaluate the use of high-frequency acoustic backscattering systems as a means of observing both internal waves and plankton. In this report, we present further results of that study. We specifically look for the effects of internal waves on the horizontal and vertical distribution of phytoplankton and

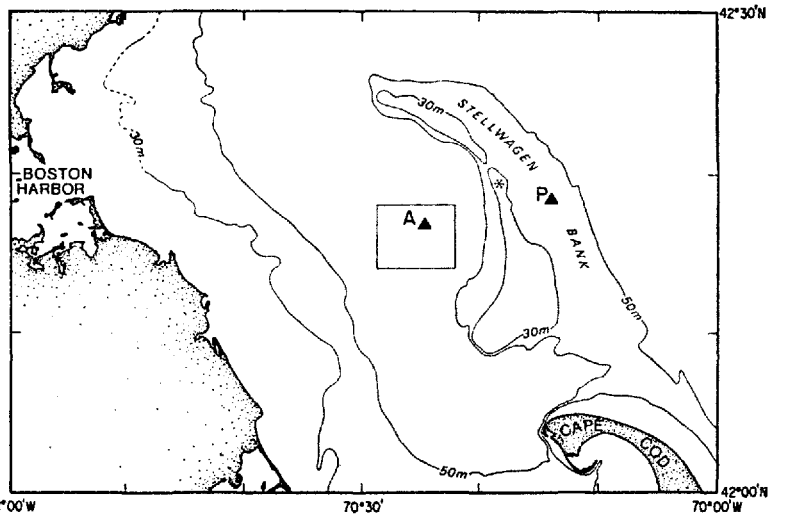

Figure 1. Chart of Massachusetts Bay showing location of moorings at Stations A and P (water depths 80 and 35 m, respectively) and area around Station A (box) within which LHPR tows were taken (see Fig. 3). Asterisk marks position where fluorometer, CTD, and acoustic records shown in Figure 10 were taken.

zooplankton; we seek to determine (1) if internal waves mechanically alter patterns of distribution; (2) if zooplankton can be regarded as passive tracers of water motion or whether their behavioral responses are sufficiently strong to allow them to significantly alter their vertical distributions with respect to vertical motion of internal waves; (3) if the above two factors affect the relationships between zooplankton species and between zooplankton and phytoplankton; and (4) if internal waves interact with the sampling design to cause biases and artifacts in the spatial distribution and relationships of plankton. This kind of localized study, utilizing high-frequency interval wave packets as a source of effects on plankton, is complementary to studies of low-frequency, internal tidal effects on plankton, such as those of Kamykowski (1974, 1976).

2. Materials and methods

a. Instrumentation. Current meters were moored at a depth of 25 m at both Stations A and P (Fig. 1); Station A also had a surface mooring carrying a thermistor chain. Details of these moorings are contained in Haury *et al.* (1979). A neutrally buoyant, free-floating vertical current meter (VCM) (Voorhis, 1968; Joyce *et al.*, 1976) was used to measure vertical and horizontal water motions during passage of the internal waves. Further description of the VCM and some of its results are in Haury *et al.* (1979). A narrow-beam (3-1/2°) 200 kHz and a 37 kHz acoustic

backscattering system (ABSS) (Orr and Hess, 1978) was used to remotely sense the internal wave field continuously during the six days of observations. The ABSS transducers were deployed on a submerged body towed at 2 m depth abeam the ship. Physical information was obtained with a CTD (conductivity, temperature, depth) sensor (Brown, 1974) augmented with occasional hydrographic casts for calibration information and for dissolved oxygen and discrete chlorophyll *a* determinations. Zooplankton samples were collected with a Longhurst-Hardy Plankton Recorder (LHPR) (Haury *et al.*, 1976) used without a net (mouth area 0.0168 m^2) and sampling at 16-second intervals. Mounted on the LHPR were an *in situ* flow-through fluorometer (Endeco Type 815) and the CTD. The lag time for flow from the fluorometer intake to the excitation chamber was 2.2 seconds; all vertical profiles of chlorophyll *a* fluorescence have been corrected for this lag. The amount of smoothing of microscale chlorophyll structure due to fluorometer intake flow field, hose turbulence, instrument response rate, and profiling speed is not known. Structure as small (<50 cm) as that reported by Derenbach *et al.* (1979) was probably not detected, but meter-scale features were easily seen.

b. Sampling strategies. The moored current meters and thermistor chain provided a continuous picture of the currents and temperature structure associated with the internal waves at Stations A and P on time scales of from less than a minute to the length of the observations (five days). Most other sampling was done in the vicinity of the mooring at Station A in order to use the current meter and thermistor records to augment the information gained from the shipborne instruments. During the five-day period, ten wave packets passed Station A; shipboard work was done in five of these packets (Fig. 2).

Two hydrocasts were taken at Station A; data from one are used here. These casts used 11 Niskin bottles spaced at 5 m intervals from the surface to 50 m. Temperature, salinity, dissolved oxygen, and chlorophyll *a* were measured from each bottle. Light penetration was estimated using a Secchi disk on four occasions.

The fluorometer was used in combination with the CTD during single vertical profiles, repeated vertical yo-yos during passage of internal waves, or with the instruments at a constant depth during packet passage. The location of the one chlorophyll fluorescence record not taken in conjunction with an LHPR tow at Station A is shown by the asterisk in Figure 1.

Nine tows with the LHPR-fluorometer-CTD combination were taken both before the arrival of internal wave packets to sample low wave conditions and at various stages of internal wave activity (Table 1). Tow locations are shown in Figure 3; three wave packets were sampled (Numbers 1, 2, 4; Table 1, Fig. 2). All tows were against the direction of the internal wave propagation at 90° to the crests except for MB-9. Headings of tows varied from 055°T to 080°T (340°-360° for MB-9); actual tracks over the bottom (Fig. 3) varied primarily because of tidal and internal wave currents. Two towing techniques were used: (1) tows at a constant depth, and

Figure 2. Five-day record of current speed, direction and temperature at 25 m measured from the mooring at Station A. The individual wave packets studied with the LHPR and/or CTD-fluorometer combination are numbered on the temperature record. Dates are based on Greenwich Mean Time (local time = GMT − 4 hr).

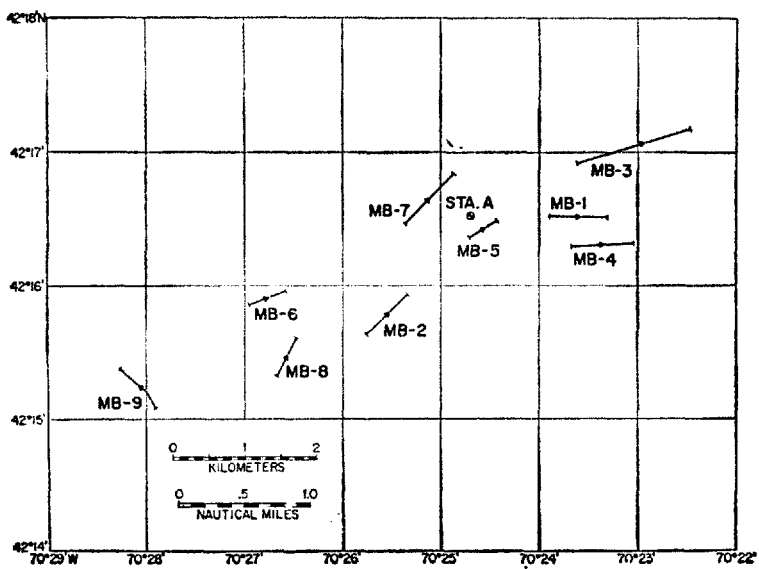

Figure 3. Position of Station A and path of LHPR tows. All positions from LORAN C fixes taken at 2- to 10-minute intervals. LHPR paths are drawn as straight lines between the start and end positions of sampling.

Table 1. Summary of Longhurst-Hardy Plankton Recorder tow information. Tow type designations are: A—constant depth at 18 m; B—following 11°C isotherm; and C—constant depth at 3 m.

Tow	Tow type	Date Aug. 1977	Time (L)	No. of samples	Tow length (m)	Mean sample length (m)	Mean volume filtered per sample (m^3)	Comments†
MB-1	A	28	0931-0952	79	1155*	14.6*	0.25	Taken in first waves of packet 1.
MB-2	A	28	1144-1205	71	950	13.4	0.23	Packet 1; sampling began after first six waves of packet had passed.
MB-3	A	28	1338-1401	63	1110	17.6	0.30	Packet 1; internal waves of much lower amplitude than during previous two tows.
MB-4	B	29	0938-0959	59	650	11.0	0.18	Taken prior to arrival of packet 2; no significant internal waves present.
MB-5	B	29	1040-1102	79	672	8.5	0.14	Sampling began just prior to leading edge of packet 2.
MB-6	B	29	1243-1303	74	600	8.1	0.14	Packet 2; sampling began after first three waves had passed.
MB-7	B	29	1403-1420	61	845	13.9	0.23	Approximately 6 km behind leading edge of packet 2; internal waves present of smaller amplitude than previous two tows.
MB-8	C	31	1340-1403	83	810**	9.8**	0.16	Sampling began just prior to leading edge of packet 4.
MB-9	B	31	1441-1502	82	850	10.3	0.17	Packet 4; towed obliquely at 60° to wave slicks until 1447, then at 45°.

† Packets numbered according to notation in Figure 2.
* Values in Haury *et al.* (1978) incorrect.
** Values in Haury *et al.* (1978, 1979) incorrect.

Table 2. Mean ($\bar{x}$), standard deviation (SD), maximum (MAX), and minimum (MIN) values for depth (Z, m), temperature (T, °C), salinity (S) and density (σ_t) for each plankton recorder tow. No salinities or densities are available for MB-1 or MB-9. Tow type designations as in Table 1.

Tow	Tow type	Parameter	$\bar{x}$	SD	MAX	MIN
MB-1	A	Z	18.3	0.560	20.5	17.0
		T	12.9	1.514	15.5	9.8
MB-2	A	Z	17.9	0.188	18.5	17.5
		T	12.4	0.830	13.8	10.4
		S	31.84	0.092	31.97	31.76
		σ_t	24.08	0.189	24.54	23.75
MB-3	A	Z	18.0	0.090	18.5	17.5
		T	9.8	0.381	10.5	9.1
		S	32.01	0.039	32.06	31.96
		σ_t	24.66	0.099	24.82	24.52
MB-4	B	Z	15.4	0.826	17.0	13.0
		T	11.0	0.110	11.2	10.7
		S	31.92	0.037	31.94	31.90
		σ_t	24.40	0.053	24.46	24.36
MB-5	B	Z	26.5	8.418	46.5	8.7
		T	11.1	1.010	14.3	8.1
		S	31.90	0.081	32.10	31.75
		σ_t	24.37	0.226	25.00	23.64
MB-6	B	Z	23.4	7.709	38.6	9.9
		T	11.0	0.872	13.0	8.6
		S	31.90	0.085	32.05	31.78
		σ_t	24.37	0.198	24.89	23.92
MB-7	B	Z	18.9	2.435	23.4	12.6
		T	11.1	0.547	12.2	9.5
		S	31.88	0.068	31.98	31.78
		σ_t	24.36	0.127	24.69	24.11
MB-8	C	Z	2.8	0.497	3.3	1.4
		T	15.1	0.463	15.7	14.1
		S	31.76	0.058	31.80	31.73
		σ_t	23.49	0.116	23.70	23.32
MB-9	B	Z	31.7	8.538	45.2	17.0
		T	11.1	0.599	12.4	9.1

(2) tows which attempted to follow a specific isotherm. At the end of two tows (MB-3 and 4), prior to shutting off the plankton recorder, oblique profiles from towing depth to 50 m and back to the surface were taken in order to obtain vertical

distributions of zooplankton and chlorophyll *a*. All tows were taken during full daylight hours to avoid problems introduced by diel vertical migration.

The internal waves caused some problems in maintaining desired depths or temperatures while towing the LHPR. During constant-depth tows, continuous corrections were needed to maintain a desired depth; the vertical water velocities associated with the internal waves were great enough to raise and lower the LHPR by as much as 10 m if left uncorrected. The rapidity of vertical water motion also made it very difficult to accurately follow a particular isotherm. An attempt to minimize this problem was made on the last tow by towing at an angle oblique to the internal wave packet, thus decreasing the apparent vertical motions. Table 2 lists depth and temperature statistics that give a measure of how well particular depths or isotherms were tracked during tows.

Ship speed was set at 1.5 kts (77 cm/sec) for tows, but speeds of the LHPR through the water during some tows varied by as much as ± 50 cm/sec due to the combination of internal wave motions and the tow cable being paid in or out to correct for depth or temperature variations.

c. Analysis. The speed and direction of the tidal currents are presented in the form of progressive vector diagrams (PVD), while the velocities associated with the internal waves are graphed as a function of time. Acoustic results have not yet been quantified, so they are presented as photographs made directly from the analog graphic records of the ABSS.

Chlorophyll *a* determinations from the hydrocasts were made by acetone extractions of glass-fiber-filtered water samples read for fluorescence on a Turner Designs fluorometer. *In situ* fluorescence of chlorophyll *a* is presented as fluorescence units (standardized fluorometer voltage output). No attempt has been made to calibrate these data to mg chl a/m^3. The LHPR samples were preserved in formalin and counts made without aliquoting. Counts were made of the nine taxonomic categories listed in Table 3; the samples were then filtered onto preweighed filters, dried at 60°C, and their dry weights determined.

Temperature, salinity, and depth information accompanying the LHPR tows were averaged for each of the 16-second sampling periods and a density calculated from the average conditions. Similarly, an average of the *in situ* chlorophyll *a* fluorescence (measured continuously but digitized during data acquisition at intervals of 3-1/3-second for the first seven tows and 1-2/3 sec for the last two tows) was calculated. Therefore, each zooplankton count is accompanied by a mean temperature, salinity, density, depth, and chlorophyll *a* fluorescence (no salinities, and therefore no densities, were available for the first and last tows).

Means, standard deviations, and indices of dispersion (Fisher, 1958) were calculated from the zooplankton counts of each tow. For each tow, Kendall's nonparametric rank correlation coefficients (Tate and Clelland, 1957) were calculated

Table 3. Species categories enumerated from the LHPR tow samples and their code numbers.

Species code	Species category
1	*Calanus finmarchicus* adults
2	*Calanus* species copepodites
3	*Centropages* spp
4	*Temora* spp
5	*Oithona* spp
6	Hyperiid amphipods
7	*Sagitta* spp
8	Appendicularians
9	Crab zooea

for the relationships between the individual species categories and between the species categories, chlorophyll *a*, and the physical parameters. A probability of 0.001 was used as a conservative marker of significant correlations and to compare the distribution of significant correlations to those expected by chance alone. Autocorrelations were calculated for all parameters to a lag of 20 using the average values for each LHPR sample. Cross-correlations between all parameters were limited to lags of from −9 to +9 (~10% of record length, Otnes and Enochson, 1978). The methods described by Blackman and Tukey (1959) were used to calculate these auto- and cross-correlations. In addition, the high sampling rate for chlorophyll *a* permitted harmonic analyses (with accompanying autocorrelations). The unfiltered data were prewhitened by finding first differences, Fast-Fourier-transformed, and each estimate recolored, using program TIMSAN of the Woods Hole Oceanographic Institution (Hunt, 1977). Since these data clearly are not random samples from a Gaussian process, these analyses are not represented as power spectra and no confidence intervals are given.

No attempt has been made to estimate horizontal patch dimensions because in all but one LHPR tow the variability in abundance of plankton was dominated by the internal waves moving large vertical gradients of abundance past the samplers or because of the difficulties of towing the samplers along an isotherm. In only a few cases were the horizontal gradients large enough to be detected above the signal of the internal waves and the noise of other factors, and only then on scales which approached that of the tow lengths.

3. Results

a. Physical environment. Bigelow (1927) reviewed the annual cycle of physical conditions in Massachusetts Bay. Greatest thermal stratification occurs in the late summer, early fall period; it is during this period that the internal waves are most easily observed. Figure 4 presents vertical profiles of temperature, salinity, oxygen, and chlorophyll *a* from a hydrocast taken near Station A on 29 August 1977. The

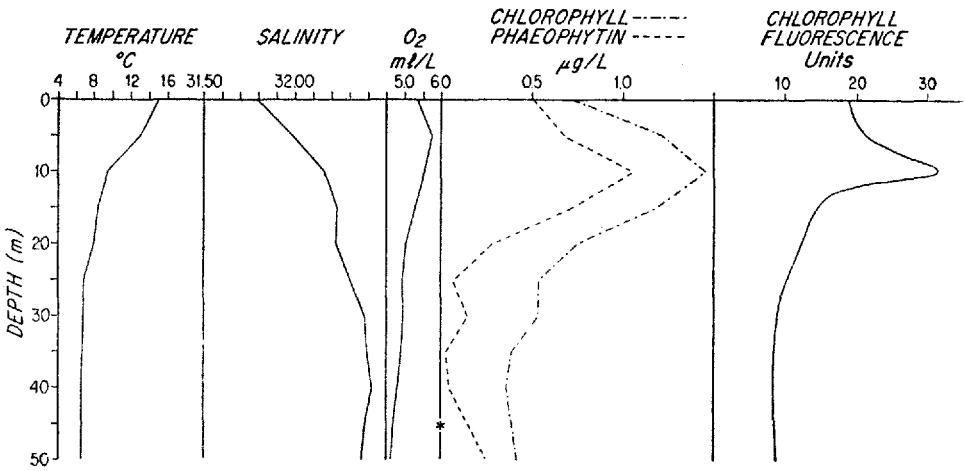

Figure 4. Profiles (temperature, salinity, dissolved oxygen, extracted chlorophyll *a*/phaeophytin and chlorophyll fluorescence) typical of Massachusetts Bay in the vicinity of Station A in the absence of internal waves. At the depth indicated by the asterisk, chlorophyll/phaeophytin values were zero; these values were ignored because we believe them to be bad.

cast was taken just prior to the arrival of internal wave packet 2 and represents the nominal conditions around Station A when undisturbed by internal waves. Density profiles closely approximated the temperature profiles, with the pycnocline occurring within the thermocline.

Winds during the seven days of observations were less than 4.2-5.2 m/sec, except for one period of several hours of winds in excess of 7.8 m/sec. Light conditions during the observations were mostly clear to hazy; heavy fog occurred on the last day. Turbidity of the water column remained relatively constant throughout the period; Secchi depths averaged about 10 m (range 7-13 m).

The tidal currents measured by the current meters at Stations A and P are shown as PVD's in Figure 5. The mean current (about 4.2 cm sec^{-1}) at Station A from NW to SE agrees in direction with the nontidal circulation shown in Bigelow (1927, Fig. 207) for the Gulf of Maine in July-August. The dominant tidal motions are east-west at Station A and northeast-southwest at Station P over Stellwagen Bank. The instantaneous speed and direction of flow from which the PVD was derived for Station A is shown in Figure 2, together with the temperature at the current meter, for the period 28 Aug.-2 Sept.

b. Nature of internal waves. The generating mechanism hypothesized for the internal wave packets is described in Haury *et al.* (1979); a new packet is generated every 12.4 h, the semidiurnal tidal cycle period. Upon formation at Stellwagen Bank, the wave packets propagate into Massachusetts Bay (heading about 240°T)

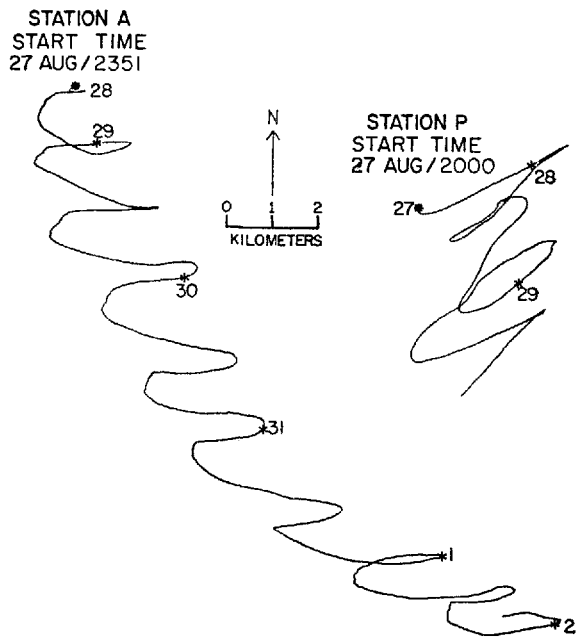

Figure 5. Progressive vector diagrams of currents measured by moored current meters at Stations A and P. Asterisks denote start of the records and each subsequent midnight (GMT). At Station P, the instrument failed on 29 August.

at a speed of approximately 60 cm/sec. The dominant waves immediately following the packet's leading edge are characterized by wavelengths of about 300 m, periods of between 8 and 10 min, and amplitudes of 10 to 20 m (maximum observed: about 30 m). The amplitudes decrease with distance behind the leading edge. There is considerable variability in wave characteristics within wave packets, including modulations in amplitude with periods of about 90 min (Fig. 3b in Haury *et al.*, 1979). Variability between packets is also considerable, as evidenced by the records shown in Figure 2.

There appears to be little or no net transport of water by the internal waves. VCM's were deployed for about 16 hr at Station A during the passage of two leading edges of packets and for 7 hr just west of Stellwagen Bank for the passage of one packet; horizontal movements of the floats during this time were due to tidal transport only, except for possible short-period back-and-forth surging as the wave packet passed.

During the low wind conditions which predominated during the observations, the internal wave packets could be seen easily from shipboard as series of alternating bands of slick and rough water. The surface roughness differences were observed

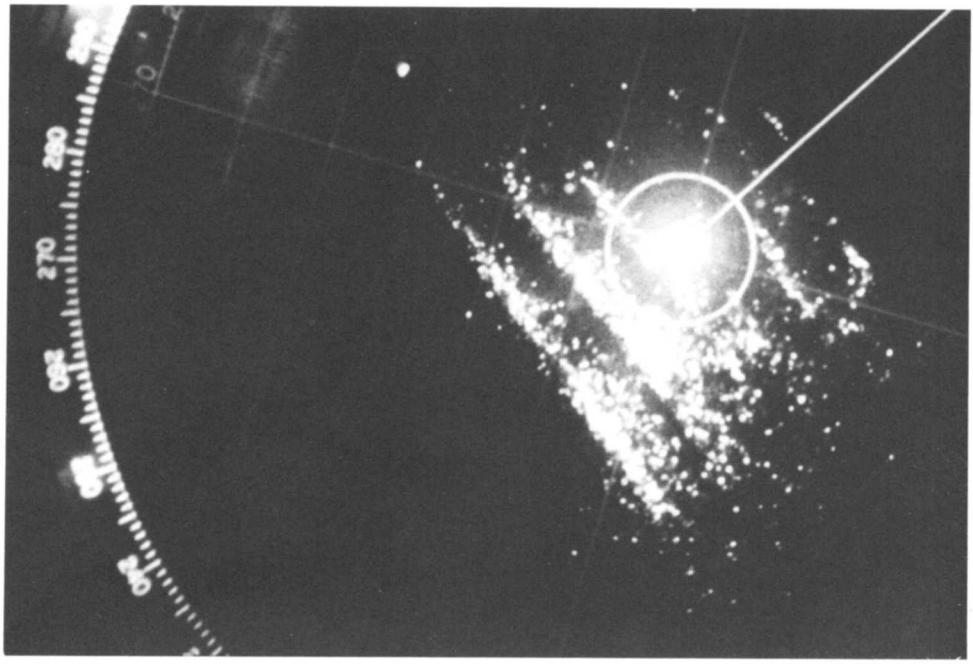

Figure 6. Ship's radar image of internal wave packet propagating southwest (240°T). North is to the top; ship's heading 050°T. Central circle (range marker) is about 370 m in radius, indicating that the wavelengths in the packet are about 340 m. Wind is from the southwest at 4.1 m sec^{-1}, causing the bands to be brighter in that direction.

on the ship's radar (Fig. 6), allowing independent estimates of propagation heading and wavelengths to be made. The bands of rough water usually occurred at and just trailing the crest of the internal wave (cold water portion). This observation agrees with those of Osborne and Burch (1980), LaFond and LaFond (1972) and with the theoretical explanation of Gargett and Hughes (1972). The banding of the sea surface usually was observable for several kilometers following the leading edge of the packet, but the distinctness and coherence of the individual bands decreased with increasing distance behind the leading edge.

The horizontal extent of the packets from northwest to southeast was of the order of 5 to 10 km. The terminal portions of the banded structures were distorted and sometimes strongly curved at angles of up to 45° to the main axis of the wave packets.

After propagating across the Bay, the packets dissipate in the shoal waters on the western side. Acoustic records from this area have shown on occasion that waves become borelike with mixing over 20 to 40 m of depth; mixing apparently can occur from the surface to near the bottom (Orr, 1982). We found no evidence of any

large internal waves heading in an easterly direction, either due to reflection of the packets or to other areas of wave generation.

Haury *et al.* (1979, Fig. 4b,c) and Orr (1982) show acoustic records and other data demonstrating that some of the individual waves in packets can become unstable and break in the deeper (80 m) parts of the Bay. In the region of breaking, substantial mixing of the water column occurs, as is evident from some of the data we present below. We have insufficient data, however, to determine the temporal or spatial occurrence of these events.

c. Internal wave effects on the biota. The passage of internal wave packets past Station A had dramatic and sustained effects on the horizontal and vertical distributions of plankton populations and on the way in which these distributions appeared in the tow records. In this section, we consider these effects: (1) for the phytoplankton; (2) for zooplankton; and (3) for the phytoplankton-zooplankton relationships. Table 4 presents a summary of the statistics upon which much of these analyses are based.

Chlorophyll a: vertical and horizontal patterns

The vertical distribution of chlorophyll *a* in the study area was characterized by a subsurface maximum at the 10.5°C isotherm. This was at a depth of between 10 and 15 m when large internal waves were not present (Fig. 4). During periods of intense internal wave activity, the chlorophyll maximum was carried passively up and down by the wave motions (Haury *et al.*, 1979, Fig. 4c) from depths of about 10 m to as deep as 40 m.

In general, the shapes of the chlorophyll fluorescence profiles were characterized by a simple monotonic increase with depth to the maximum, then a slower monotonic decrease to undetectable levels at depths between 30 and 50 m. Figures 4, 7a and 7b show typical profiles unaffected by internal wave motions. Details of this generalized shape varied both in time and space and seemed to be related to the internal wave history of the parcel of water, particularly the localized occurrence of overturning caused by breaking internal waves. Figure 7b, a profile taken 75 min after the profile of Figure 7a, shows considerable detail and small inversions; both of these profiles were taken at the same location prior to the arrival of internal wave packet 3. During overturning, secondary maxima in chlorophyll occur (Fig. 7c,d). These apparently persist for a considerable length of time after the overturning event; Figure 7e shows a profile with a strong double peak taken halfway (6 hr) between packets. Broad shoulders above the chlorophyll maximum sometimes were observed (e.g., Fig. 7f); these may be secondary peaks which have been diffused. Differences among fluorescence profiles taken between packets may reflect the localized nature of breaking events, *e.g.*, contrast Figures 7a and b with 7e and f.

Horizontal distributions of chlorophyll along isotherms were relatively uniform;

Table 4. Mean ($\bar{x}$), standard deviation (SD), maximum (MAX), and minimum (MIN) values for chlorophyll *a* (CHLA, fluorescence units), zooplankton dry weight (DWT, mg m^{-3}) and species categories (no. m^{-3}; codes defined in Table 3) for each plankton recorder tow.

				Species category								
		CHLA	DWT	1	2	3	4	5	6	7	8	9
MB-1	$\bar{x}$	25.2	40.7	*	121.8	12.1	32.4	*	23.4	15.8	20.7	1.6
	SD	5.7	15.87		46.42	22.12	50.34		17.50	10.11	30.82	4.66
	MAX	33.0	89.3		258.3	100.0	229.0		73.9	44.0	128.6	28.6
	MIN	14.3	11.2		28.3	0.0	0.0		0.0	0.0	0.0	0.0
MB-2	$\bar{x}$	30.1	50.9	3.6	204.8	22.4	16.2	11.9	10.3	24.6	22.6	1.4
	SD	3.8	18.99	7.54	171.54	61.72	30.65	33.79	14.71	18.06	20.74	3.03
	MAX	38.0	101.7	58.3	816.7	311.5	142.9	200.0	56.5	106.7	92.9	17.4
	MIN	22.5	23.0	0.0	0.0	0.0	0.0	0.0	0.0	0.0	0.0	0.0
MB-3	$\bar{x}$	30.0	14.7	0.6	40.5	0.2	21.9	0.4	2.2	31.3	1.3	0.2
	SD	27.3	6.20	1.57	17.97	0.86	10.58	1.26	4.73	12.78	2.47	0.85
	MAX	34.6	49.1	8.6	109.1	3.2	54.5	6.4	33.3	64.5	10.0	3.3
	MIN	25.1	7.7	0.0	9.7	0.0	0.0	0.0	0.0	6.3	0.0	0.0
MB-4	$\bar{x}$	31.9	42.1	2.6	158.6	*	38.0	1.7	4.8	7.9	*	1.4
	SD	0.9	11.93	4.23	80.18		22.07	2.70	6.11	7.48		2.54
	MAX	33.7	77.0	16.7	321.0		128.6	11.8	22.7	30.0		10.0
	MIN	30.2	25.0	0.0	45.0		0.0	0.0	0.0	0.0		0.0

MB-5	$\bar{x}$	30.8	20.3	0.7	12.4	0.6	35.6	2.7	6.4	6.9	*	2.4
	SD	7.4	9.95	2.87	13.84	2.90	47.09	5.83	14.01	8.83		5.65
	MAX	41.2	67.5	18.2	60.0	21.4	292.8	33.3	100.0	50.0		35.7
	MIN	12.1	5.7	0.0	0.0	0.0	0.0	0.0	0.0	0.0		0.0
MB-6	$\bar{x}$	48.8	29.2	0.1	1.6	2.7	25.6	4.3	2.6	17.9	0.6	3.3
	SD	4.7	21.42	0.62	3.34	4.93	28.41	12.58	4.45	17.97	2.03	5.95
	MAX	56.7	135.0	5.3	14.3	25.0	154.5	100.0	22.2	100.0	11.1	25.0
	MIN	36.2	0.0	0.0	0.0	0.0	0.0	0.0	0.0	0.0	0.0	0.0
MB-7	$\bar{x}$	45.0	19.0	0.5	16.6	0.9	63.3	3.9	4.7	20.5	0.8	0.9
	SD	2.2	7.35	1.45	14.67	4.47	63.80	4.05	6.38	12.51	2.12	1.93
	MAX	48.6	51.1	7.1	100.0	33.3	328.6	14.3	33.3	73.7	11.1	7.7
	MIN	36.5	8.1	0.0	0.0	0.0	0.0	0.0	0.0	0.0	0.0	0.0
MB-8	$\bar{x}$	13.1	13.7	*	8.2	33.4	51.4	*	1.8	0.6	12.5	1.4
	SD	1.8	24.05		25.92	46.23	98.35		6.68	2.53	18.48	3.74
	MAX	17.5	193.3		200.0	300.0	733.3		50.0	15.4	150.0	21.4
	MIN	10.6	1.4		0.0	0.0	0.0		0.0	0.0	0.0	0.0
MB-9	$\bar{x}$	35.1	58.6	0.7	286.7	0.5	15.3	2.8	16.9	59.7	0.1	4.1
	SD	6.1	24.10	2.19	165.14	2.05	13.81	4.04	11.65	34.76	0.59	6.76
	MAX	54.5	121.0	15.0	761.1	15.0	58.3	17.4	45.5	183.3	5.3	35.0
	MIN	25.7	24.3	0.0	61.5	0.0	0.0	0.0	0.0	7.1	0.0	0.0

* Not present

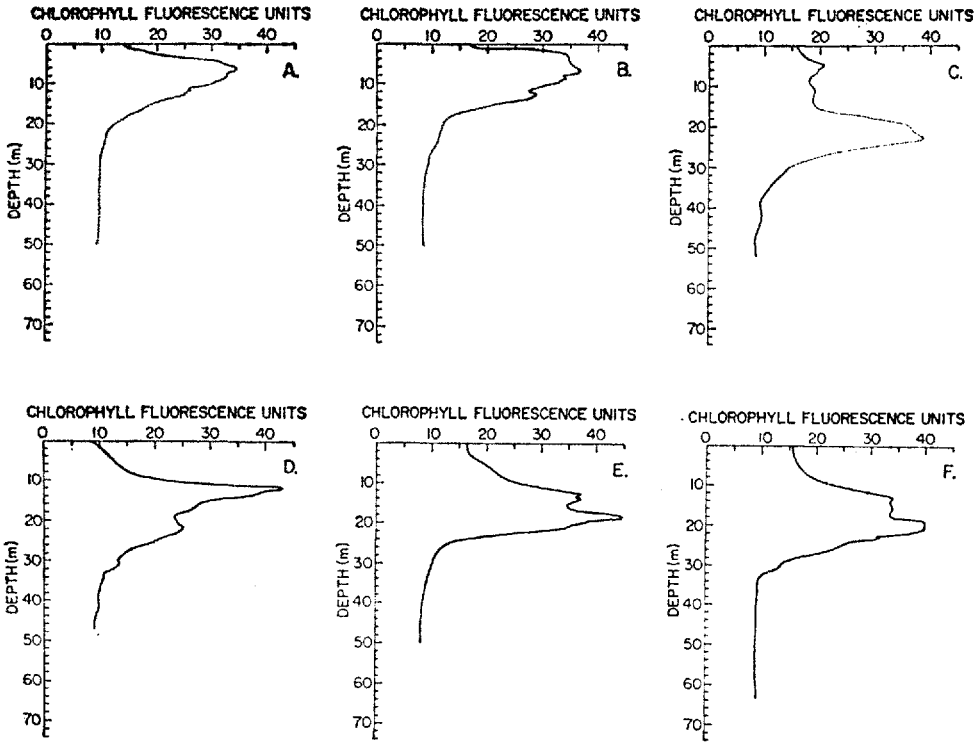

Figure 7. Chlorophyll fluorescence profiles from different times with respect to internal wave packet passage near Station A. (a) 90 min prior, (b) 15 min prior, and (c) 30 min after arrival of Packet 3; (d) quiescent region after passage of Packet 1 following LHPR tow MB-3; (e) 6 hr after Packet 3; (f) 2 hr after arrival of the first packet shown in Figure 2 (0330 GMT 28 Aug.).

Figure 4c in Haury *et al.* (1979) shows a region in the chlorophyll maximum only about 10% higher than the background level in the maximum. These higher values persisted for approximately 15 min as the ship drifted southwest a distance of 400 m. The true dimensions of this low-gradient patch cannot be determined because the ship was being advected an unknown amount by the internal wave circulation. Another example of the horizontal uniformity of chlorophyll *a* at Station A is shown in Figure 8a by the chlorophyll fluorescence trace from tow MB-4, taken following the 11°C isotherm prior to internal wave packet arrival. The uniform gradient of chlorophyll (3 fluorescence units/km) was uncorrelated with temperature, salinity, density, or depth of tow (Table 5) and probably represents a scale of patchiness much larger than the tow length (650 m). The small variations greater than about 1% of the mean and with scales of 10's of meters were caused by overshoots in depth by the LHPR while making depth corrections to follow the

11°C isotherm. Autocorrelations of chlorophyll using the data acquired at the 3-1/3 sec rate and with the trend over the entire tow length removed showed no significant correlations after zero lag. Because the lag interval represents about 2 m of travel, there appeared to be no characteristic scale of pattern between about 4 m and 400 m. The harmonic analysis was also flat, showing no peaks due to characteristic scales of patchiness (Fig. 8b).

Chlorophyll variability measured at a constant depth, either by towing or by remaining stationary for long periods of time, was dominated by the presence of internal waves. In Figure 9a, the chlorophyll trace from constant-depth tow MB-1 (Table 1) is in distinct contrast to the chlorophyll record of MB-4 (Fig. 8a). The autocorrelation for chlorophyll (Fig. 9b) has the first zero crossing at about lag 4, corresponding to a length of ~60 m, thus giving a wavelength of the internal waves of about 240 m. The harmonic analysis of the MB-1 chlorophyll trace (Fig. 9c) shows a distinct peak in variance at a period of about 5 min. These wavelength and period estimates are doppler-shifted shorter than the true values because the instruments were being towed into the wave packet.

Because of the deep chlorophyll maximum, the depth placement of the chlorophyll sensor strongly affects the variability of the signal. Figure 9a shows only a single peak of chlorophyll with the passage of each wave, because the chlorophyll maximum never passed the sensor. Figure 10a illustrates a chlorophyll trace when the chlorophyll maximum passed the sensor: there is a double peak in chlorophyll for every internal wave; the separation of peaks depends on the amplitude of the particular passing wave. This record, taken at a depth of about 17 m over Stellwagen Bank (water depth about 25 m, Fig. 1), shows internal waves of smaller amplitude and shorter period than in the deep water at Station A.

Another feature of this record is of interest and is best discussed in reference to the acoustic record taken at the same time (Fig. 10b). Superimposed on the overall chlorophyll trends are sporadic small peaks associated with similar temperature fluctuations (Fig. 10a). These appear to be due to mixing and are associated with regions of intense backscattering of sound in the ABSS record. In general, throughout the entire record, the short periods of small thermal and chlorophyll variability coincide with the acoustic backscattering intensity. The appearance in the acoustic record of "double-braided structures," that is, the two bands of intense backscattering which appear to intertwine (after 0930 local time, Fig. 10) are the manifestation of the last stages in the breaking and subsequent mixing, decay, and restabilization of internal waves (Orr, in review). The CTD-fluorometer combination was not at the correct depth to pass through these regions directly; these instruments' records, however, show an abrupt change in character in temperature and chlorophyll at about 0932, coincident with the appearance of the braided structure. This is a result of the smaller amplitude of the internal waves and possible increased mixing.

a)

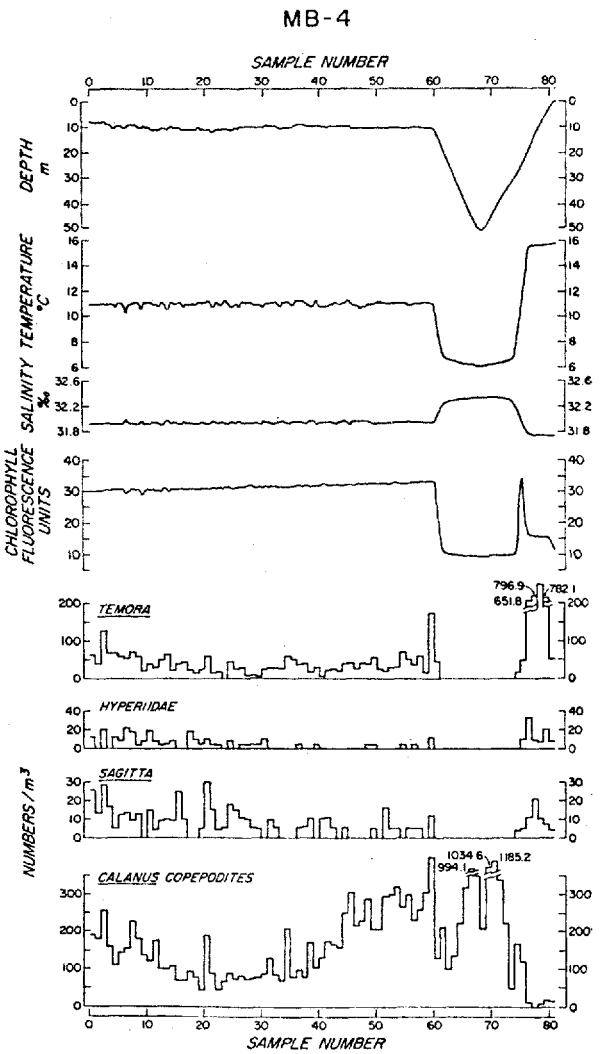

Figure 8. Horizontal LHPR/CTD/fluorometer transect prior to arrival of Packet 2 at Station A. (a) Physical, chlorophyll fluorescence and zooplankton species data vs. sample number. See Table 1 for other tow information. (b) Harmonic analyses of chlorophyll fluorescence for horizontal section (ending at LHPR sample 60).

Attempts to follow isotherms to look at variability unassociated with the vertical displacement of internal waves were marginally successful. Considerable variability was introduced by the difficulty in maintaining the instruments at the desired isotherm. The greater the amplitude of the internal waves, the more difficult it was to follow an isotherm closely. While this technique removed autocorrelations and

b)

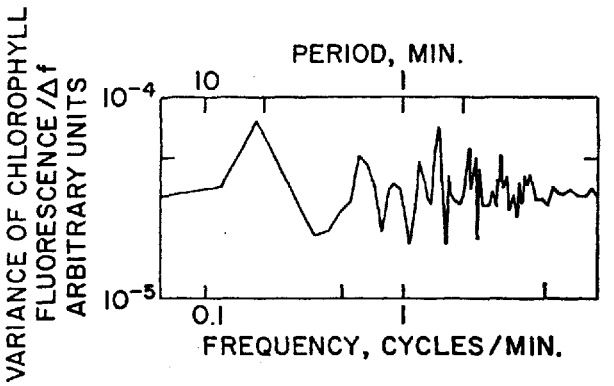

peaks in the harmonic analyses due to the internal waves, spurious autocorrelations and harmonic peaks were introduced. Figures 11 and 12 illustrate these effects for tows MB-7 and MB-9. Tow MB-7 (Fig. 11a) was through a set of internal waves with small vertical amplitudes (see depth profile in Fig. 11a and tow statistics in Table 2). The temperature and chlorophyll variability was great, with the autocorrelation for chlorophyll fluorescence (Fig. 11b) showing a first zero crossing at a lag of 6 (20 sec, about 17 m). The harmonic analysis (Fig. 11c) showed no peak related to internal waves; between periods of one and ten minutes, the variance tends to be flat, presumably because isotherm-following reduced the longer-period variability. Tow MB-9 (Fig. 12), towed obliquely through a vigorous packet, showed a first zero crossing in the chlorophyll fluorescence autocorrelations (Fig. 12b) at lag 204 (340 sec or 230 m travel); this lag is clearly not due to internal

Table 5. Kendall Rank Correlation Coefficients (τ) for the relationship of chlorophyll *a* fluorescence to temperature (T), salinity (S), density (σ_t), and depth of tow (Z) for all LHPR tows. The value of τ required for significant correlation at $p = 0.001$ for each tow is given. Values of τ with $p \leqslant 0.001$ are asterisked.

	T	S	σ_t	Z	$\tau: p = 0.001$
MB-1	−.876*	§	§	.451*	± .230
MB-2	−.729*	.724*	.734*	.133	± .250
MB-3	.863*	−.867*	−.864*	.248	± .270
MB-4	.087	−.105	.071	.125	± .275
MB-5	−.380*	.242*	.344*	.196	± .230
MB-6	−.037	−.165	−.006	−.094	± .260
MB-7	−.438*	.350*	.457*	.019	± .275
MB-8	−.785*	.651*	.775*	.427*	± .230
MB-9	−.467*	§	§	.267*	± .230

§ Salinity and density not available.

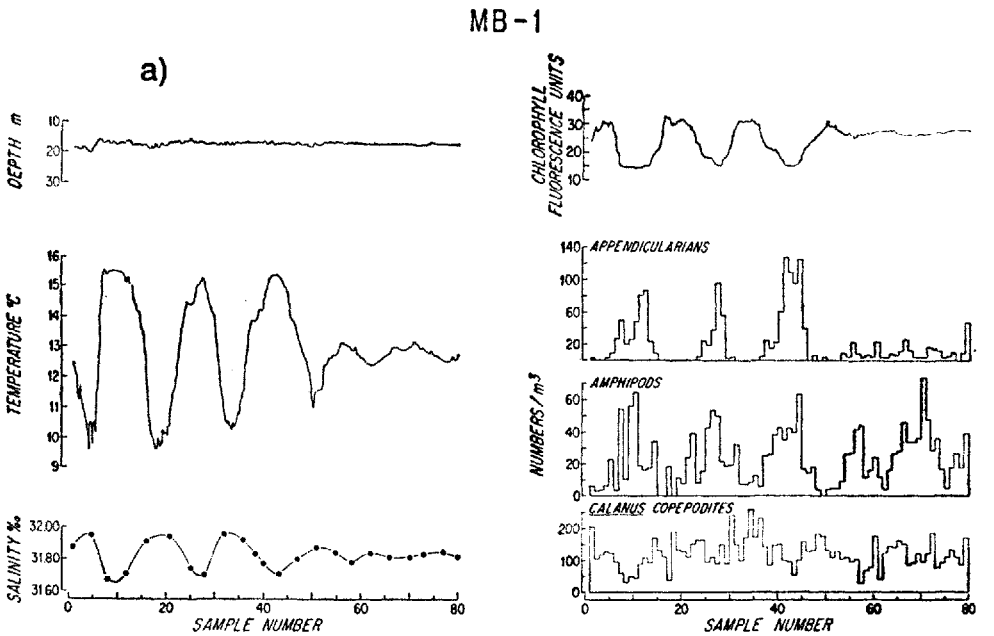

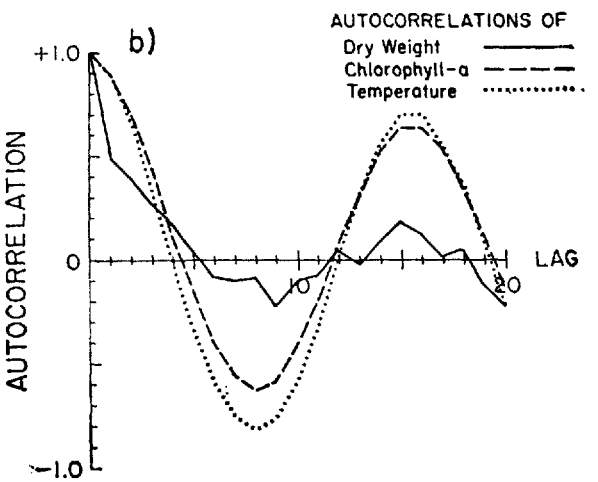

Figure 9. Horizontal LHPR/CTD/fluorometer transect through the first five waves of Packet 1. (a) Physical, chlorophyll fluorescence and zooplankton species data vs. sample number. See Table 1 for other tow information. (b) Autocorrelations of zooplankton dry weight, chlorophyll fluorescence and mean temperature using values averaged to each LHPR sample. (c) Harmonic analysis of chlorophyll fluorescence.

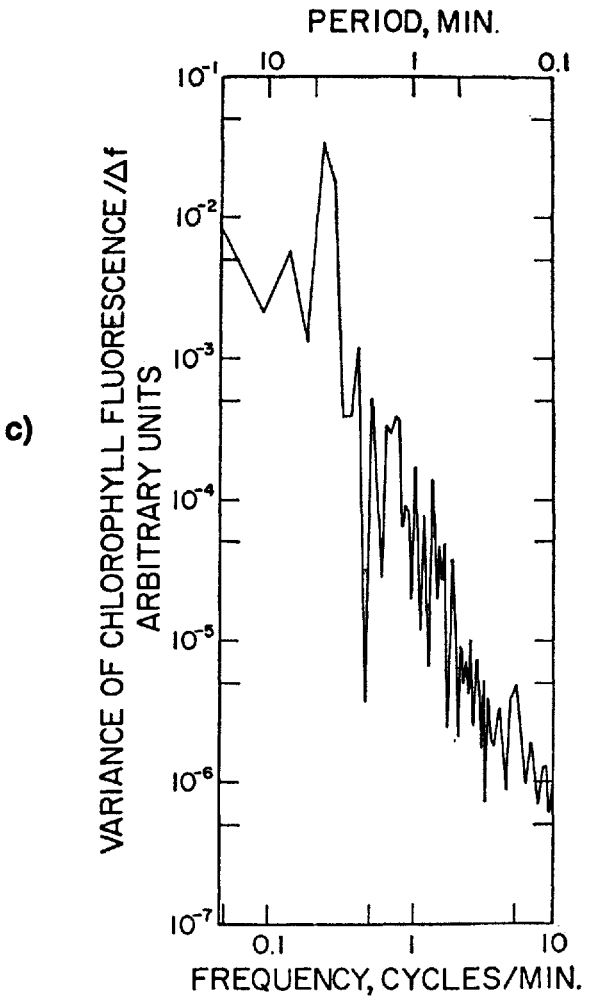

waves. It appears to be due to the slow change in average temperature from the target 11°C isotherm evident throughout the tow (Fig. 12a). This resulted in the positive correlation of chlorophyll *a* fluorescence with temperature. The harmonic analysis of MB-9 (Fig. 12c) lacks a peak related to the expected doppler-shifted wave period at about four minutes. Contrast these records with those for MB-4 (Fig. 8), an isotherm-following tow with virtually no internal waves present, and MB-1 (Fig. 9), a constant-depth tow through strong internal waves. Had we done a perfect job of isotherm following, we would have expected the harmonic analysis of MB-7 and MB-9 to look like that of MB-4. Autocorrelations and harmonic analyses for chlorophyll records from the other two isotherm-following tows (MB-5 and MB-6) in high-amplitude internal waves were similar to MB-9.

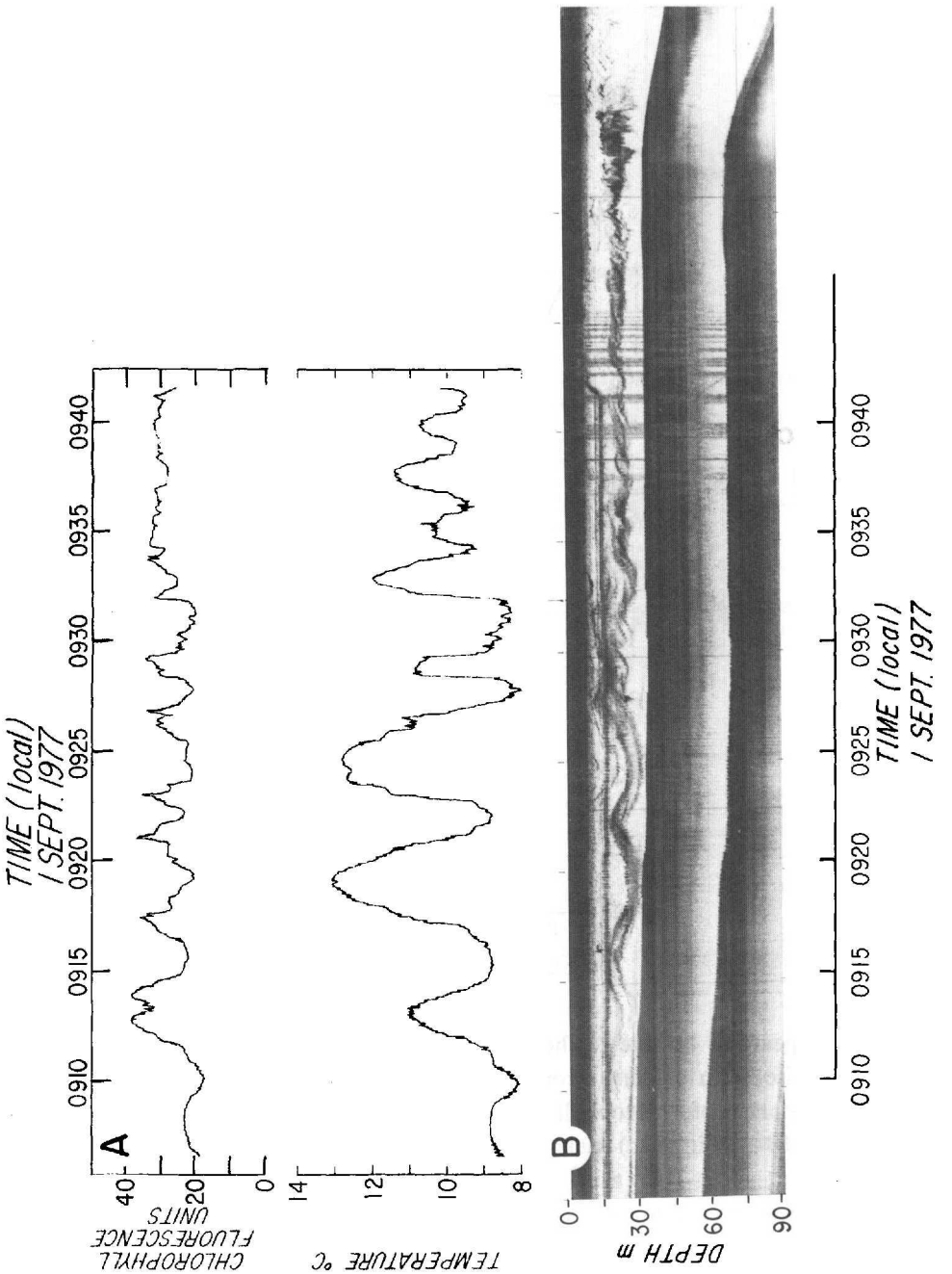

Figure 10. CTD/fluorometer record (a) and acoustic record (b) of internal waves passing the drifting vessel over Stellwagen Bank at position shown by asterisk in Figure 1. Note the large (~0.25°C), rapid (less than one minute) fluctuations of the temperature record in the regions where acoustic backscattering indicates mixing has occurred. The CTD/fluorometer forms the continuous dark trace at about 17 m in (b).

Zooplankton: vertical and horizontal patterns

Figure 13 shows the vertical distributions of temperature, chlorophyll fluorescence, and representative zooplankton species and dry weight obtained on two different days at Station A. The profile for MB-3 (Fig. 13a) was obtained about 2 hr after the passage of Packet 1 and for MB-4 (Fig. 13b) in the leading edge (first trough) of Packet 2. Despite the great differences in absolute abundance between the two days, the species are divided into two distributions—those associated with the mixed layer and thermocline, and those occurring mostly in the thermocline and below. As with the chlorophyll *a* vertical profiles discussed in the previous section, the differences between zooplankton profiles suggest that internal wave packets may affect vertical distributions in ways other than to merely displace them vertically. The profiles in the packet leading edge (MB-4) show a clear separation of the two groups at the well-defined, but greatly depressed, thermocline. In contrast, MB-3 has a less well-defined thermocline and mixed layer; several of the mixed-layer species (*e.g.*, numbers 4, 6, 7) extend down through the 7°C to 15°C region. This difference could be a result of mixing processes associated with shear instabilities. The chlorophyll profile for MB-3 has a marked secondary maximum, as do profiles for temperature and chlorophyll (Fig. 14) taken 33 min before the profiles in Figure 13a; these features suggest mixing was taking place.

What has been said about horizontal distributions of chlorophyll applies equally well to the zooplankton. Plankton recorder tows MB-1, MB-3, MB-4, MB-8 and MB-9 (Figs. 9a, 15, 8a, 16 and 12a, respectively) illustrate the variety of patterns that occur with and without the influence of internal waves. Long horizontal trends are evident in some tows (Figs. 8a, 11a and 12a), particularly those following isotherms where the internal wave effects do not obscure them. For tows at a constant depth through internal waves, the horizontal patterns observed depend on the depth of the tow relative to the vertical distributions of individual taxa. Tow MB-8 (Fig. 16), taken at a constant depth of about 3 m, graphically illustrates the patterns that can emerge. A schematic representation of the 200 kHz acoustic record is included in Figure 16 to show the vertical wave motions needed to interpret the horizontal patterns. In general, cooler water at the wave crests brings the deeper-living species to the surface (*e.g. Calanus* copepodites); mixed-layer species (appendicularians, *Temora, Centropages*) show a variety of patterns which are dependent on differences in their vertical distributions and on the amplitude of the waves and whether or not the waves have broken. For example, appendicularians and *Centropages* start to become more abundant at about sample 8 as the first trough of the packet deepens and the temperature at 3 m slowly cools. *Temora* increases at about sample 18 as the other two begin to decline in abundance. At sample 20, a sudden decrease in temperature is associated with the appearance of heavy acoustic backscattering at the LHPR depth, possibly due to turbulence associated with shear instabilities. No marked peak in total zooplankton dry weight corresponds to this increase in back-

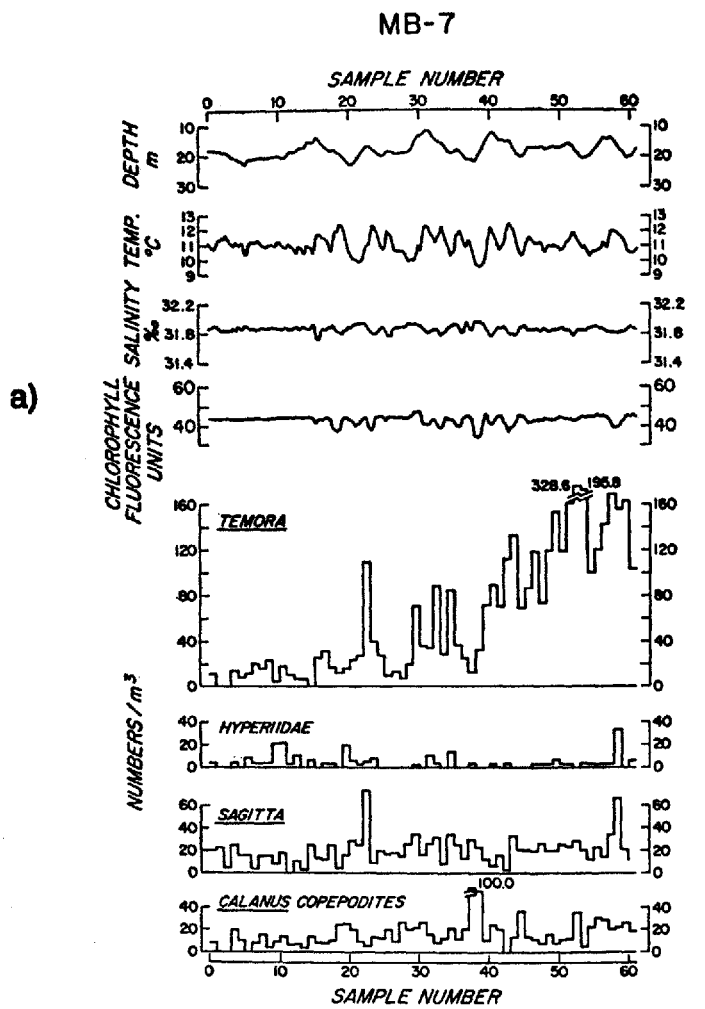

Figure 11. Isotherm-following LHPR/CTD/fluorometer transect through Packet 2. (a) Physical, chlorophyll fluorescence and zooplankton species data vs. sample number. See Table 1 for other tow information. (b) Autocorrelations and (c) harmonic analysis of chlorophyll fluorescence using data acquired every 3-1/3 sec.

b)

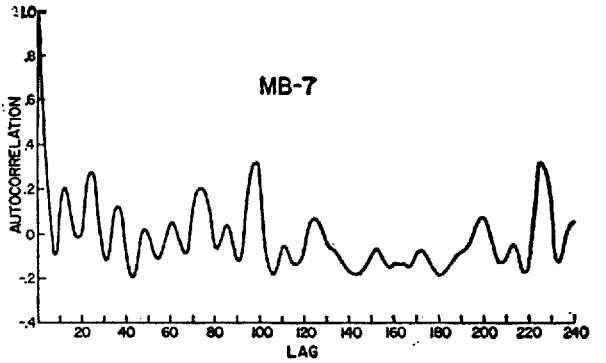
MB-7
AUTOCORRELATION
1.0
.8
.6
.4
.2
0
-.2
-.4
20
40
60
80
100
120
140
160
180
200
220
240
LAG

c)

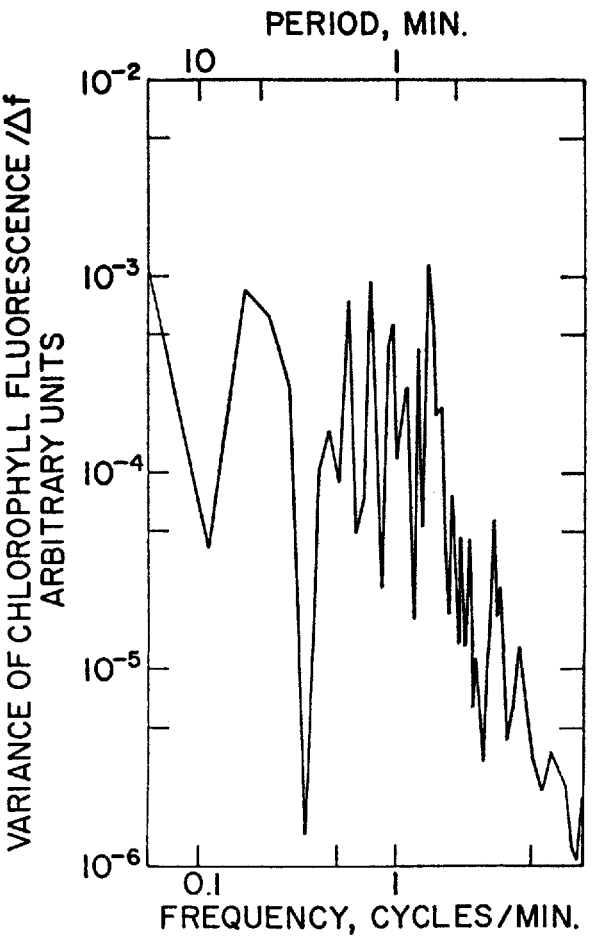
PERIOD, MIN.
10
1
10^{-2}
10^{-3}
10^{-4}
10^{-5}
10^{-6}
VARIANCE OF CHLOROPHYLL FLUORESCENCE /Δf
ARBITRARY UNITS
0.1
1
FREQUENCY, CYCLES/MIN.

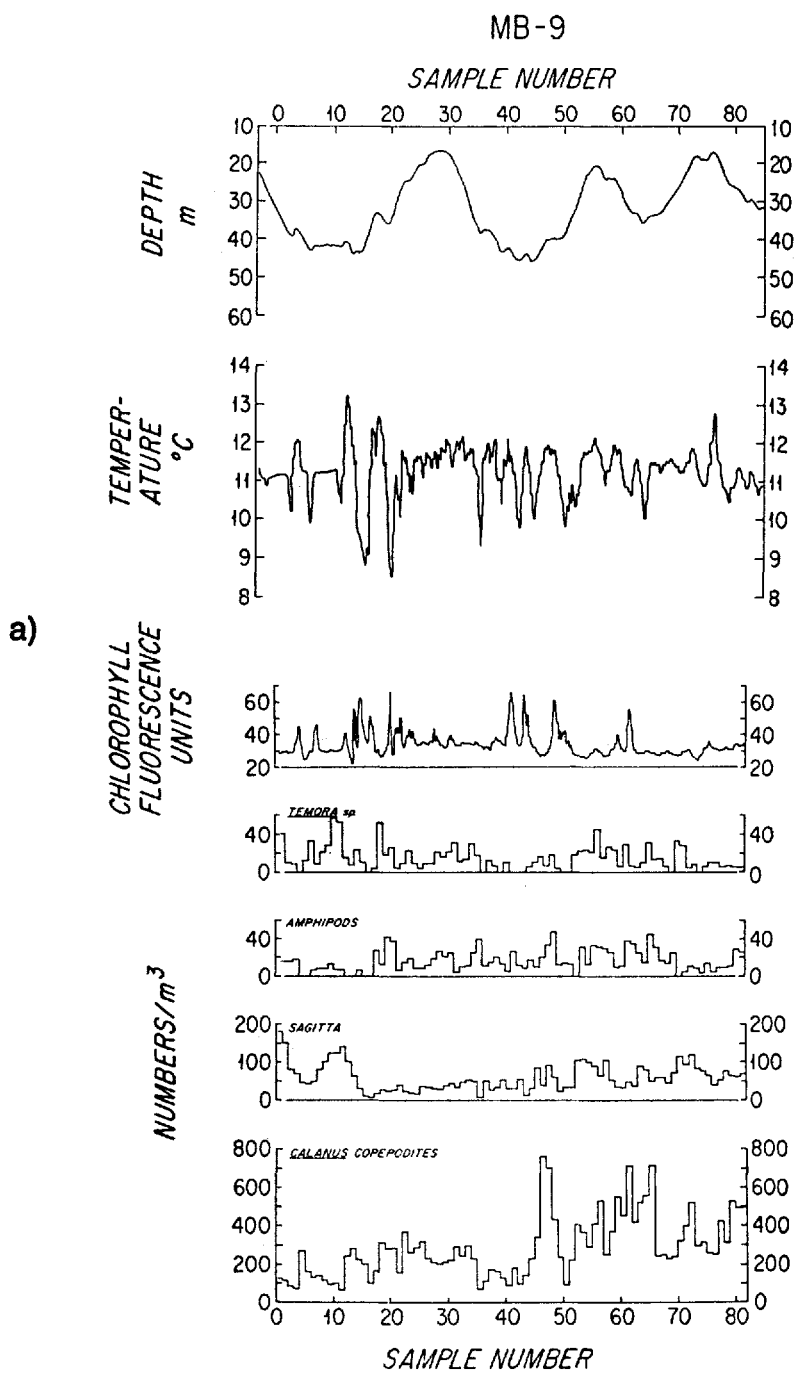

Figure 12. (a-c) As in Figure 11 except for Packet 4, and chlorophyll values used in (b) and (c) acquired every 1-2/3 sec. (d) Acoustic backscattering record (200 kHz) and (e) zooplankton dry weight profile. LHPR path traced by black line; vertical bars mark start and end of LHPR samples. Dry weight biomass peaks denoted by letters.

b)

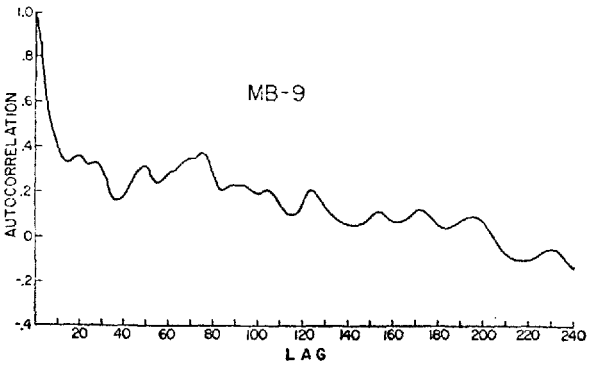
MB-9
AUTOCORRELATION
1.0
.8
.6
.4
.2
0
-.2
-.4
20
40
60
80
100
120
140
160
180
200
220
240
LAG

c)

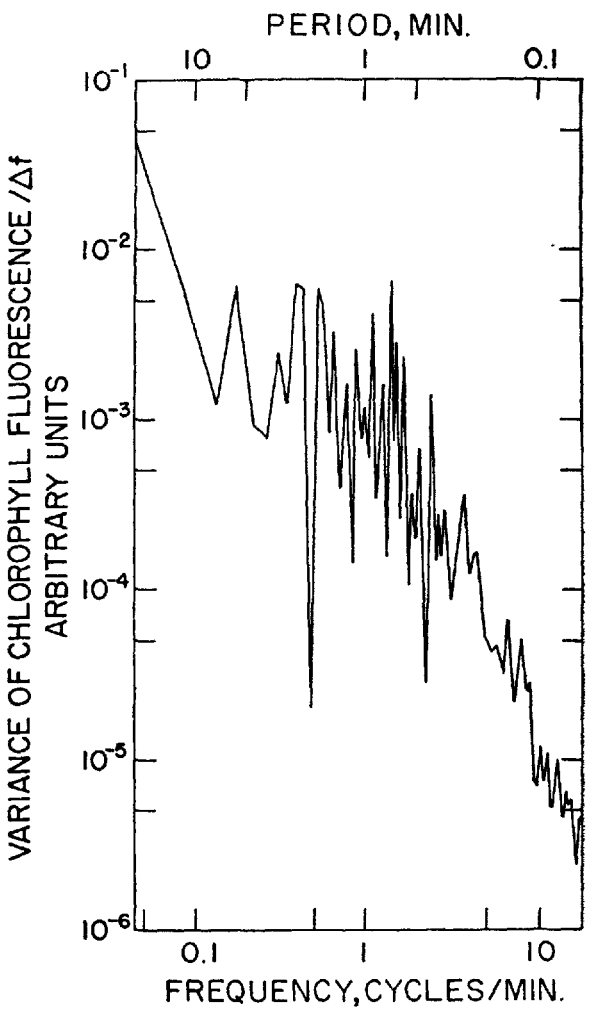
PERIOD, MIN.
10
1
0.1
VARIANCE OF CHLOROPHYLL FLUORESCENCE /Δf
ARBITRARY UNITS
10^{-1}
10^{-2}
10^{-3}
10^{-4}
10^{-5}
10^{-6}
0.1
1
10
FREQUENCY, CYCLES/MIN.

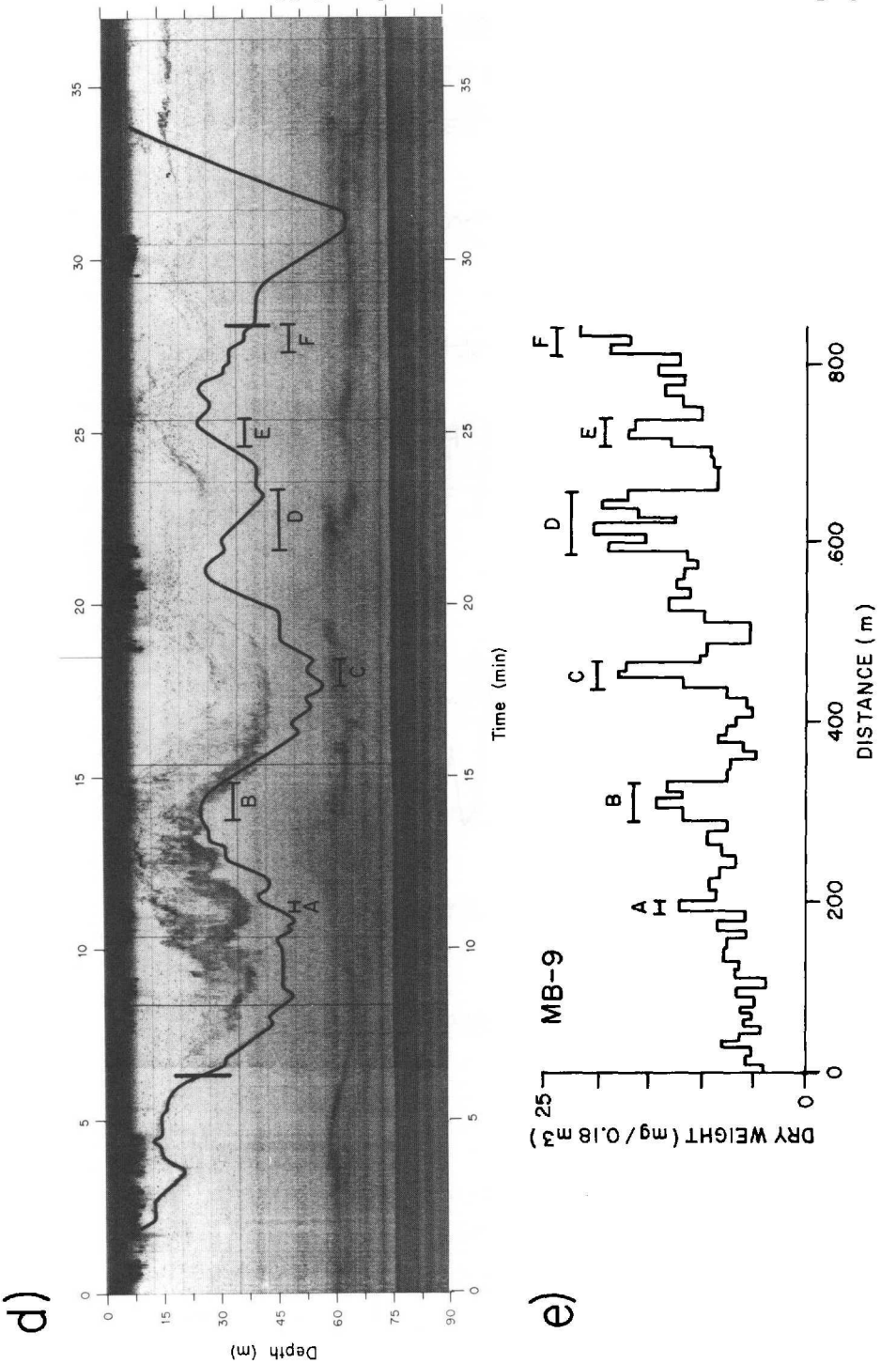
d)
Depth (m)
Time (min)
A
B
C
D
E
F
e)
MB-9
DRY WEIGHT (mg / 0.18 m3)
DISTANCE (m)

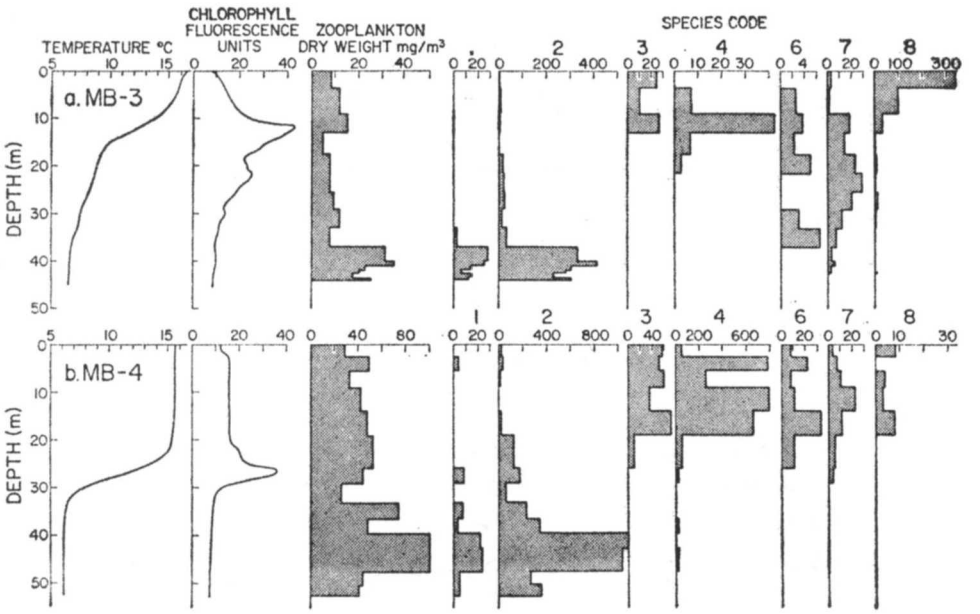

Figure 13. Vertical profiles of temperature, chlorophyll fluorescence, zooplankton dry weight and species (codes given in Table 3) taken on the oblique upward section of (a) LHPR tow MB-3 and (b) MB-4.

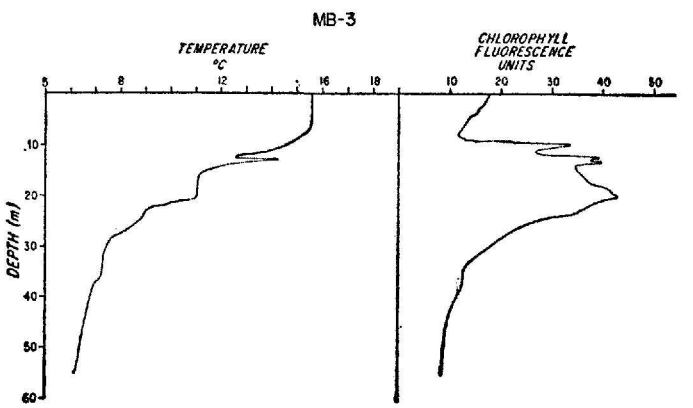

Figure 14. Vertical profiles of temperature and chlorophyll fluorescence taken 33 min before the profiles shown in Figure 13a. Inversions in temperature and chlorophyll profiles around 10 m depth suggest overturning has occurred.

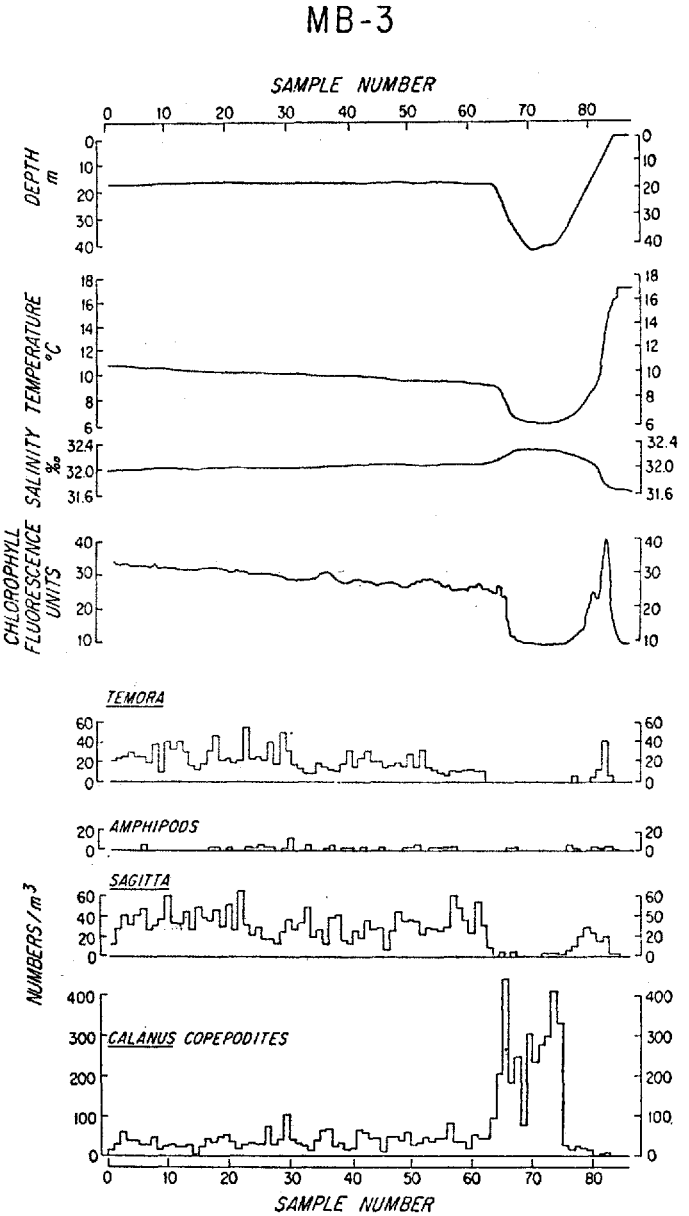

Figure 15. Horizontal LHPR/CTD/fluorometer transect taken at position shown in Figure 2 following passage of Packet 1. (a) Physical, chlorophyll fluorescence and zooplankton species data versus sample number. See Table 1 for other tow information.

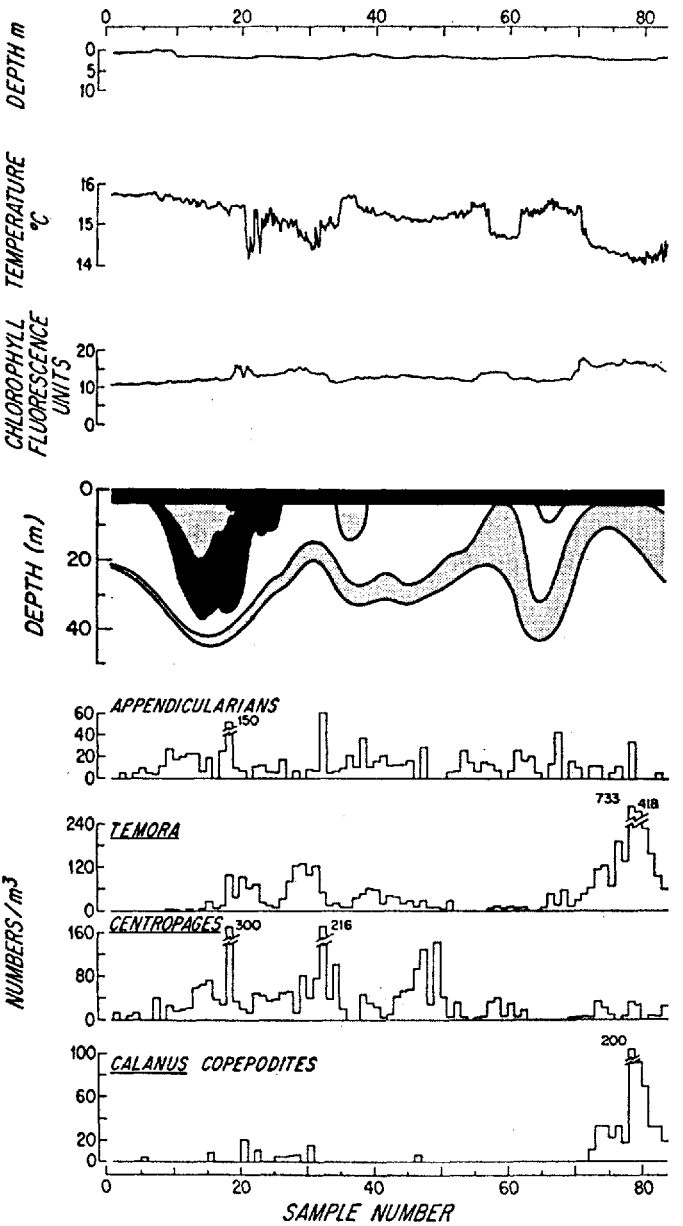

Figure 16. Near-surface, horizontal LHPR/CTD/fluorometer transect through first three waves of Packet 4. The fourth graph from the top is a schematic representation of the acoustic record taken simultaneously with the LHPR transect. The darkness of shading is proportional to backscattering intensity except for the black band between the surface and 5 meters.

a)

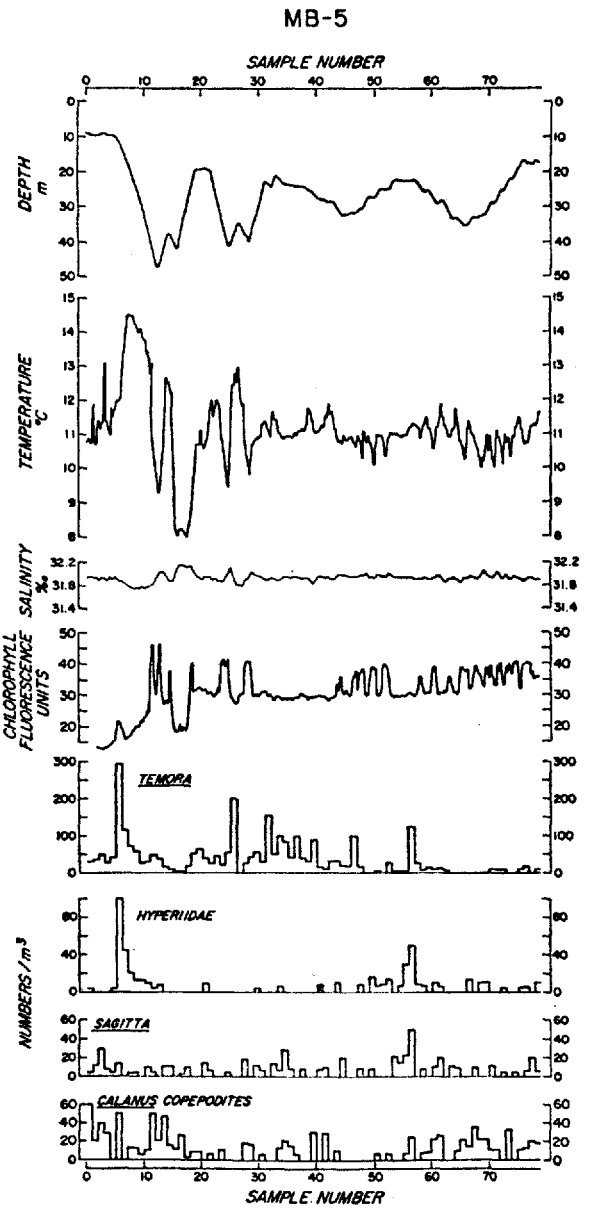

Figure 17. Isotherm-following LHPR/CTD/fluorometer transect through Packet 2. (a) Physical, chlorophyll fluorescence and zooplankton species data versus sample number. See Table 1 for other tow information. (b) Acoustic backscattering record (200 kHz) and zooplankton dry weight profile. LHPR path marked by the black line and dark trace in acoustic record; vertical bars mark start and end of LHPR samples. Dry weight biomass peaks denoted by letters and horizontal bar.

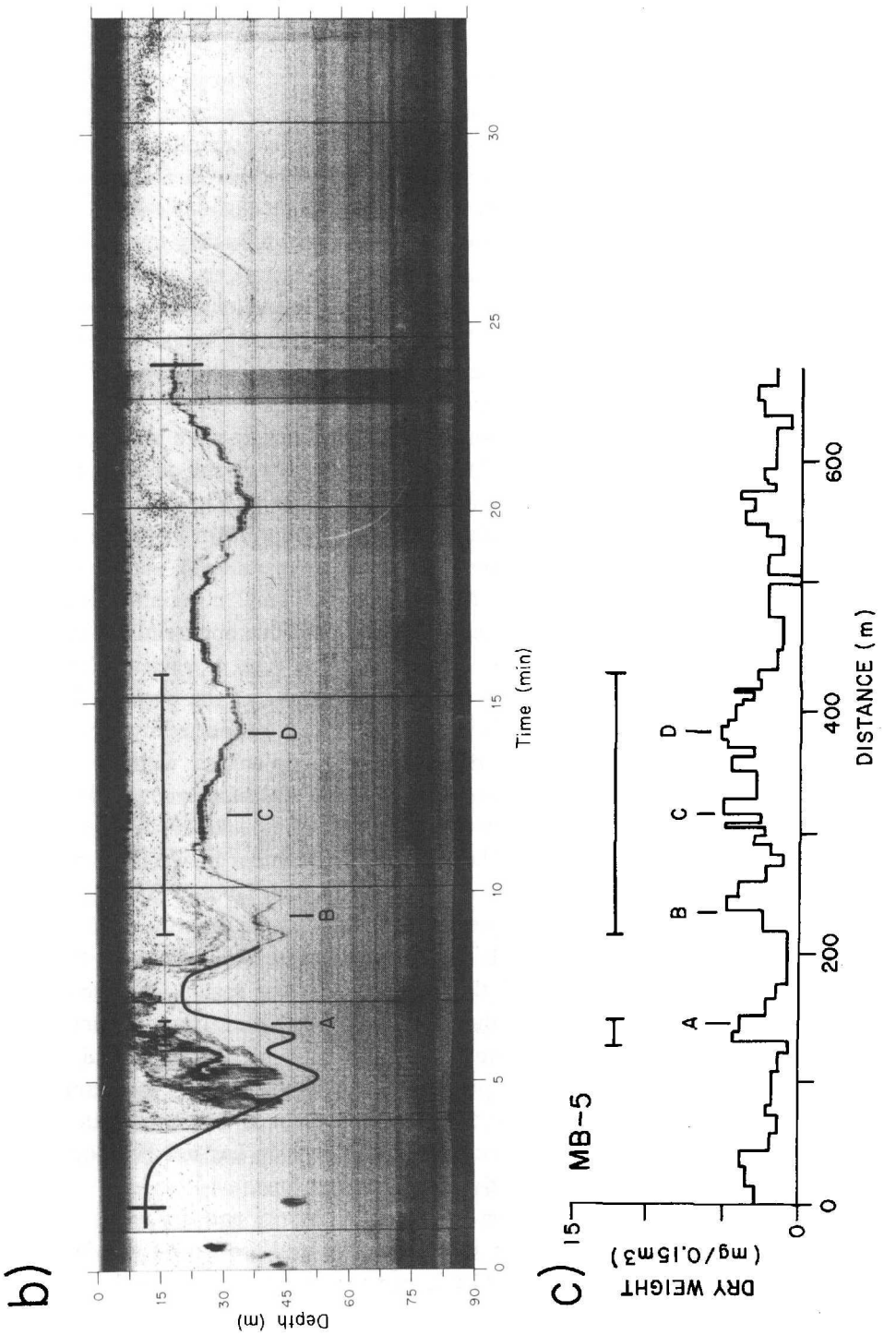
b)
Depth (m)
0
15
30
45
60
75
90
Time (min)
0
5
10
15
20
25
30
A
B
C
D
c)
MB-5
DRY WEIGHT
(mg/0.15m3)
15
0
A
B
C
D
0
200
400
600
DISTANCE (m)

scattering. A warming of temperature, with backscattering still present, corresponds with a decrease in *Temora*, which then increases again as the next wave crest approaches the LHPR and the temperature decreases. A *Centropages* increase tends to lag the *Temora* increase and, by sample 35, all three abundances are low. Later peaks in *Temora* and *Centropages* appear related to wave amplitude, but appendicularians do not. Clearly, a large fraction of the variations in abundance result from processes associated with the internal waves.

Acoustic records obtained during two of the isotherm-following tows (MB-5 and MB-9, Figs. 17b and 12d) showed the LHPR in the record and thus can be used to: (1) interpret the LHPR record in terms of two-dimensional vertical scattering structure, as was inferred above for MB-8, and (2) directly relate backscattering with captured zooplankton abundance. There appear to be four types of acoustic scattering sources in the 200 kHz records: (1) the discrete "blobs" (*e.g.*, those at 0-2 min, Fig. 17b) assumed to be fish schools because they were more evident in the 37 kHz records (Orr, 1981); (2) the small discrete, point-source scatterers, assumed to be zooplankton or small fish (in the troughs of Fig. 17b, 20-25 min); (3) the dark, generally uniform, undulating bands at about 75 m in Figure 17b and 60 m in Figure 12d, due to euphausiids (*Thysanoessa rauschii*, sampled with a meter net at 1600L, 1 Sept.); and (4) the black or dark grey "curtainlike" scattering at 4-10 min in Figure 17b and 8-17 min in Figure 12d, due apparently to turbulent microstructure and its associated temperature gradients (Orr, in review; Curtin and Mooers, 1975; Kraus *et al.*, 1973) in the first two waves of the packets. That the cause for this last type of scattering is not zooplankton is supported by a qualitative comparison of the tow records for dry weight of zooplankton with the acoustic record of backscattering intensity. The profiles of dry weight for each tow are shown below the acoustic records (Figs. 12e and 17c), with the peaks in biomass marked in both for comparative purposes. The only good agreement between biomass and intensity of scattering is for a portion of the peak biomass labelled B in Figure 12d and e; this peak however does not persist for the length of time the samples were taken in the dark scattering band. It should be noted that despite peak B, which appears to occur in the middle of the intense scattering region, the records for temperature, chlorophyll, and individual taxa from this region (sample numbers 22 to 35, Fig. 12a) show greater uniformity than any other part of the record. This is an indication of mixing, as well as perhaps better tracking of the isotherm. Even for the overall profile, it appears that zooplankton biomass and backscattering intensity are, if anything, inversely related. This relationship has not been quantified because the acoustic data are qualitative at the present time.

Autocorrelations to a lag of 20 for taxonomic categories and dry weights exhibit a dichotomy of patterns related to constant-depth and isotherm-following tows. Tow MB-1 (Fig. 9b and 18a) and MB-2, constant-depth tows through strong internal waves, show a periodicity caused by the internal wave passage. Tow MB-4

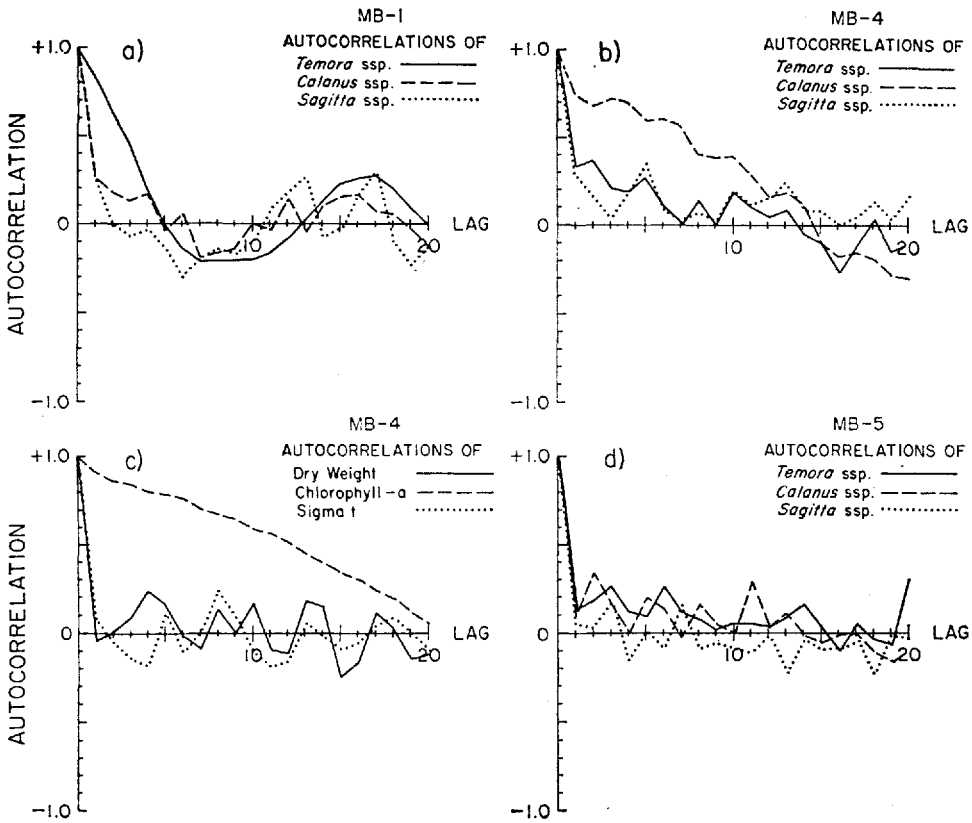

Figure 18. Autocorrelations to lags of 20 for three zooplankton species for (a) MB-1, (b) MB-4, and (d) MB-5. (c) Autocorrelations for density, zooplankton dry weight biomass, and chlorophyll fluorescence for MB-4.

(Fig. 18b), an isotherm-following tow through negligible internal waves, shows lagged autocorrelations related to the long trends of abundance that are clear in Figure 8a. These data were not detrended prior to calculating autocorrelations. The superimposed periodicity of about 4 lags in the autocorrelations (and seen in the abundance profiles, Fig. 8a) are caused by the small variations in depth of tow during isotherm following, as shown by the autocorrelation for σ_t (Fig. 18c). Autocorrelations for taxonomic categories in another isotherm-following tow, MB-5 (Fig. 18d), are representative for this type of tow when made in strong internal waves. Autocorrelations fall to insignificant levels ($p>0.05$) at lags greater than one. No characteristic scale of pattern smaller than the tow length is discernible in the data for any species, probably because of the noise introduced by the towing technique.

Table 6. Kendall Rank Correlation Coefficients (τ) for the relationship of zooplankton dry weight to temperature (T), salinity (S), density (σ_t), and depth of tow (Z) for all LHPR tows. Values of τ required for significant correlation at $p = 0.001$ for each tow are the same as in Table 5. Values of τ with $p \leqslant 0.001$ are asterisked.

	T	S	σ_t	Z
MB-1	.425*	§	§	−.249*
MB-2	.107	.000	−.087	−.275*
MB-3	−.300*	.286*	.292*	−.112
MB-4	.063	−.259	.297*	.110
MB-5	.061	−.045	−.056	−.062
MB-6	.034	−.010	−.031	−.106
MB-7	−.071	.061	.067	.218
MB-8	−.627*	.525*	.619*	.311*
MB-9	.077	§	§	−.245*

§ Salinity and density not available.

The relationships between zooplankton (individual taxonomic categories and dry weight) and the physical variables (temperature, salinity, density, and depth), using Kendall's rank correlation coefficient τ (Tables 6 and 7), were clear. The tows at constant depth (MB-1,2,3,8) showed far more significant correlations at the 0.001 level (41 of 128, 32%; $p<<0.005$ that this number of significant correlations was due to chance alone) than the isotherm-following tows (8 of 168, 4.3%; $p > 0.30$ that this number of significant correlations was due to chance alone). Of special note in the latter tows, species with obvious long-term trends in abundance (*e.g.*, MB-7, *Temora*, Fig. 11a and MB-4, *Calanus* copepodites, Fig. 8a) showed no significant correlations to physical variables. For the constant-depth tows, the relationship (magnitude and sign of the correlation coefficient) between a species and the physical parameters is a function of the species' vertical distribution, the depth of tow, and the amplitude of the internal waves. Thus, for example, *Calanus* copepodites are always negatively correlated with temperature, while *Temora* is positively correlated with temperature on the three deep horizontal tows (MB-1,2,3) and negatively correlated on the shallow tow (MB-8). These relationships are expected from their vertical distributions (Fig. 13a,b).

Cross-correlations between zooplankton and density (temperature for MB-1) for the constant-depth tows showed the expected peak positive and negative correlations at lags of approximately the doppler-shifted wavelength of the internal waves (*e.g.*, MB-2, Fig. 19a,b). These relationships were much less clear, however, for MB-3, a tow with little internal wave activity, and MB-8, the surface tow. In contrast, the lagged cross-correlations for isotherm-following tows showed no consistent discernible patterns (*e.g.*, Fig. 19c,d, MB-5), corroborating the conclusion that biotic variations on these tows were not related to measured physical variability.

Relationships between abundances of individual zooplankton species categories and between species categories and total dry weight/sample for each tow using Kendall's τ were strongly affected by the towing technique. Constant-depth tows showed many significant correlations at the 0.001 level: 34% of all correlations for categories to dry weight ($p<0.005$ due to chance alone); 23% for categories to categories ($p<0.005$), with most of the significant correlations occurring in MB-1, MB-2 and MB-8, the tows with the clearest internal wave dominance. Horizontal tows through internal waves which are vertically displacing species with different vertical distributions would be expected to show such high correlations between the species. There was no consistent occurrence of significant correlations, however, between the same pairs of categories in any of the tows. This is in part due to the interactions of tow depth, internal wave amplitude, and the vertical distribution of the animals. In isotherm-following tows, significant correlations between categories and dry weight were reduced to 19% ($p<0.005$ due to chance alone) and between categories to 6% ($p>0.9$), again with no consistency among categories. The tow with negligible internal wave activity, MB-4, which might be expected to have the clearest evidence for real biological relationships, showed no significant correlations at the 0.001 level between categories; only one category (*Calanus* copepodites, the numerical dominant) was significantly correlated with dry weight.

Cross-correlations were calculated only between the three taxonomic categories which were abundant in all nine tows (*Calanus* copepodites, *Temora* spp and *Sagitta* spp) and between these categories and total dry weight/sample. For the constant-depth tows, the cross-correlations were all dominated by the presence of internal waves, just like the cross-correlations of categories to density. Cross-correlations for the isotherm-following tows, in general, showed no discernible or significant lags.

Chlorophyll-zooplankton relationships

The relationships between the vertical profiles of chlorophyll *a* fluorescence, total zooplankton dry weight, and zooplankton taxonomic categories are shown in Figures 13a and b. The dry weight biomass peak below the thermocline in both tows is due almost entirely to immature stages of *Calanus finmarchicus*. At these depths and values of fluorescence, there is little actual chlorophyll present (see Fig. 4). Since no tows were taken at night, we have no evidence to show whether or not these copepods vertically migrated into the shallower waters to graze on the high chlorophyll present there.

The relationships shown in Figure 13 would be expected to remain constant to one another during internal wave passage unless mixing occurred or the plankton responded actively to the passage of the waves by changing their depth relative to particular isotherms. We have suggested in the previous two sections that there is some evidence for mixing affecting vertical distributions; however, our data are too sparse to support a discussion of the possibility of active response.

Table 7. Kendall rank correlation coefficients (τ) for the relationships of species categories (defined in Table 3) to temperature (T), salinity (S), density (σ_t), and depth of tow (Z) for all LHPR tows. Values of τ required for significant correlation at $p = 0.001$ are the same as in Table 5. Values of τ with $p \leqslant .001$ are marked with an asterisk.

		Species category								
TOW		1	2	3	4	5	6	7	8	9
MB-1†	T	§	−.238*	.603*	.431*	§	.417*	.257*	.633*	.347*
	Z	§	.161	−.451*	−.219	§	−.194	−.162	−.397*	−.174
MB-2	T	−.065	−.237	.328*	.406*	−.024	.250*	.230	.258*	.074
	S	.039	.188	−.173	−.301*	.014	−.225	−.254*	−.165	−.017
	σ_t	.061	.233	−.298*	−.393*	.033	−.242	−.227	−.240	−.061
	Z	−.096	−.181	−.106	−.033	−.067	−.037	.095	.031	−.012
MB-3	T	−.263	−.204	−.017	.394*	.183	−.096	.078	−.147	.070
	S	.243	.178	.023	−.405*	−.171	.086	−.068	.131	−.059
	σ_t	.256	.195	.017	−.397*	−.181	.095	−.074	.141	−.063
	Z	.000	−.166	.000	.090	.000	.000	−.121	.000	.000
MB-4	T	−.000	−.106	§	−.074	−.176	−.020	−.001	§	−.117
	S	−.064	−.195	§	−.165	.159	.140	−.129	§	−.196
	σ_t	.097	.085	§	.052	−.110	−.083	.110	§	−.192
	Z	.052	−.085	§	−.164	.128	.032	−.155	§	.125

MB-5	T	−.025	−.002	.123	.178	−.028	.076	.027	§	.030
	S	−.031	.022	.011	−.054	.010	−.104	.009	§	.001
	σ_t	.011	.001	−.088	−.141	.027	−.076	−.008	§	−.019
	Z	.036	−.011	−.232*	−.151	.010	−.150	−.136	§	−.196
MB-6	T	.086	−.078	.080	.318	.016	−.071	−.139	.154	.031
	S	.034	.137	.003	−.173	−.028	.011	.208	−.124	.086
	σ_t	−.065	.099	−.066	−.296*	−.028	.055	.179	−.149	−.009
	Z	−.038	.004	−.013	−.172	.001	−.020	−.113	.067	−.176
MB-7	T	.139	−.169	.064	.114	.056	−.041	−.122	.071	.178
	S	−.224	.207	−.040	−.023	−.041	−.038	.148	−.122	−.136
	σ_t	−.158	.180	−.063	−.086	−.060	.013	.118	−.093	−.177
	Z	.027	.030	−.109	−.268	.110	.054	−.061	.050	−.222
MB-8	T	§	−.478*	−.160	−.547*	§	−.023	−.251*	.159	−.187
	S	§	.450*	.213	.470*	§	−.020	.233*	−.119	.195
	σ_t	§	.472*	.163	.537*	§	.013	.248*	−.156	.187
	Z	§	.265*	.296*	.312*	§	−.151	.103	−.033	.132
MB-9†	T	−.012	.098	.046	.275*	.239*	.082	.097	.089	.211
	Z	−.272*	−.209	−.089	−.111	−.170	−.062	−.126	.135	−.390*

† Salinity and density not available.
§ Species not present or not counted.

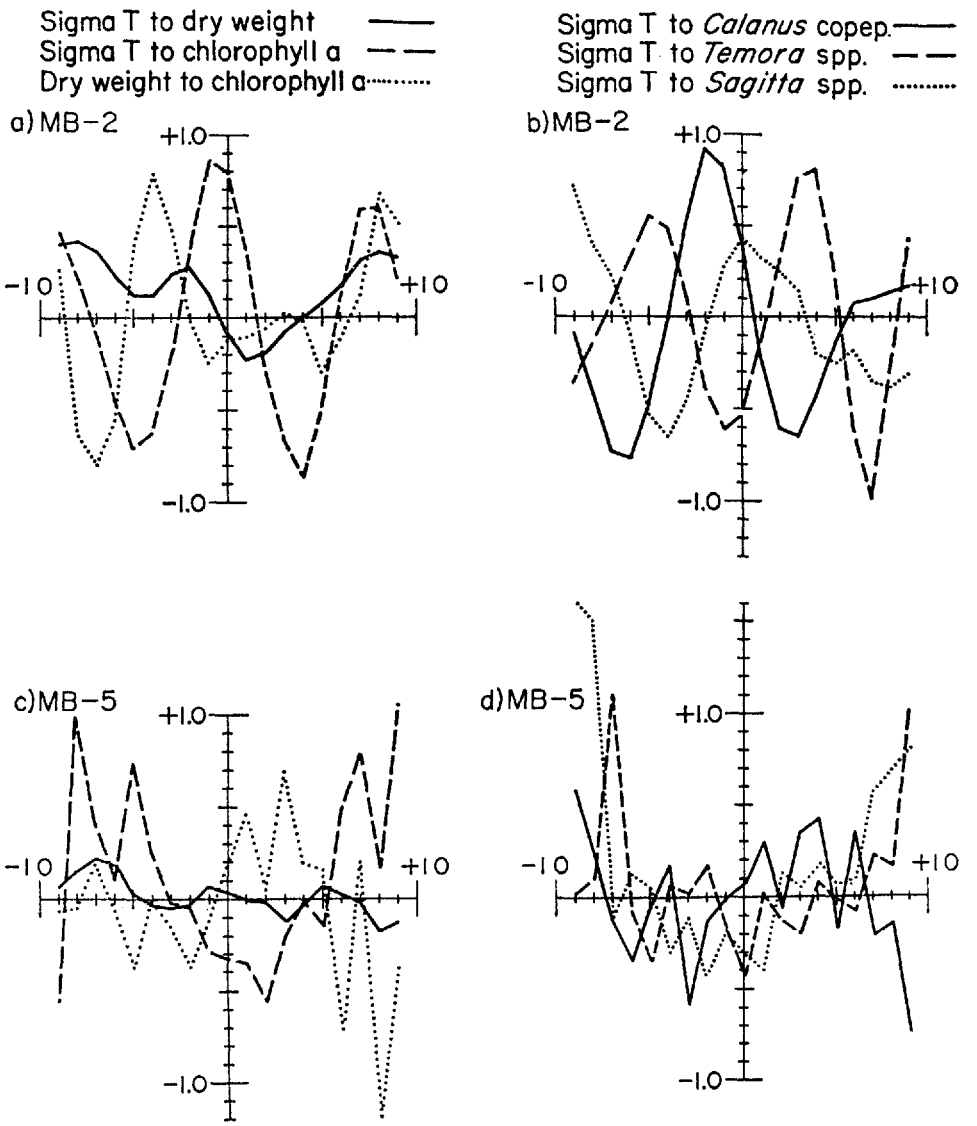

Figure 19. Cross-correlations to lags of ± 9 between density, chlorophyll fluorescence, zooplankton dry weight biomass, and three zooplankton species for (a,b) MB-2 and (c,d) MB-5.

As with the analysis of species categories, the testing of horizontal relationships between zooplankton and chlorophyll *a* used the three most abundant categories in all nine tows: *Calanus* copepodites, *Temora* spp, and *Sagitta* spp. Total zooplankton dry weight/sample was also compared to chlorophyll *a*.

Three of the four constant-depth tows showed significant ($p<0.001$) Kendall correlation coefficients for the relationship of chlorophyll *a* to zooplankton dry weight/sample. Two of these were negative (MB-1 and MB-3) and one positive (MB-8, the surface tow). Of the five isotherm-following tows, there was only one significant coefficient, a negative relationship for MB-6.

For the relationship of individual species categories to chlorophyll *a*, the same pattern as for dry weight occurred. The four constant-depth tows had a total of 12 significant correlations out of a possible 34 (35%), while the isotherm-following tows had 8 of 45 (18%) significant. Significant correlations are present primarily when internal wave effects are the dominant cause of abundance variations. Isotherm following reduces some of the significant variations, but introduces correlations due to tow depth variability.

4. Discussion

The high-frequency internal waves in Massachusetts Bay are similar to internal waves present in many continental-shelf regions of the world (*e.g.*, Apel *et al.*, 1976). They are not as energetic or as large as those in the Andaman Sea (Osborne and Burch, 1980) and Sulu Sea (Apel *et al.*, 1980; Holbrook *et al.*, 1980) but are probably more energetic than most: for example, those off the coast of Southern California (*e.g.*, Ewing, 1950; Carsola and Callaway, 1962; Armstrong and LaFond, 1966). Because the internal waves in Massachusetts Bay occur as simple, predictable packets, we were able to observe the effects of this kind of internal wave on plankton and to study the interactions of these waves with sampling techniques. We expect that our results would apply to other areas, including the open ocean (except for the importance of overturning, which may be reduced), where similar internal waves (*e.g.*, 5-10 min period, 15-30 m amplitude) are found. We also expect, however, that in open ocean situations, where internal wave fields may be much more complicated, the spatial patterns and processes resulting from plankton-internal wave interactions will be more difficult to sample adequately and interpret. The observations also allow inferences to be made concerning the role internal waves may play in patterning distributions of organisms and in nutrient regeneration and production processes in the ocean's surface layers.

The most obvious result of the sampling in Massachusetts Bay is the clear dependence of the observed patterns of chlorophyll and zooplankton, as well as their relationships to each other and to physical parameters, on the towing technique used. These effects should be present, therefore, in studies of small-scale distributions utilizing any device which takes sequential samples (*e.g.*, LHPRs, pumps, underwater cameras, and video systems) either horizontally or by following isotherms. Without some way to obtain vertical distributions nearly synoptically with the horizontal, any interpretation of horizontal patterns in terms of biological, phys-

ical, or sampling artifact causes will always be suspect where strong internal waves are present. Acoustic backscattering, while valuable in providing a picture of internal wave motions, by itself does not give the information on species' vertical distributions needed to interpret horizontal patterns. If mixing processes are sufficiently intense, scattering may be dominated by them; backscattering due to variations in the vertical distribution of biomass will be obscured.

The sampling protocol we used was not adequate to determine if species were actively moving vertically in reaction to internal wave displacements. This might occur, for example, if their preferred depths were determined by light and not temperature. Organisms' active reaction to internal waves becomes more important with longer-period waves which give the organisms time to accomplish depth adjustments. This works to the advantage of the investigator, however, because isotherms are more easily tracked and because consistent lags between plankton abundance and physical factors would be more easily detectable.

Patterns of abundance on scales much larger than the wavelength of the internal waves appear to be detectable by either of the techniques used in this study. These may be real biological changes or artifacts due to the effects of longer-period fluctuations associated with the internal waves, such as the modulations of the waves making up packets (Haury *et al.*, 1979) or the even larger-scale monotonic changes in the average depth of isotherms through time as shown in Figure 2 and in Haury *et al.* (1979, Fig. 3).

A factor complicating the interpretation of chlorophyll fluorescence patterns with *in situ* fluorometers is the effect of the rapidly varying light regime due to internal wave displacements on the fluorescence yield of phytoplankton cells. Since calibration samples for absolute chlorophyll were not obtained during the fluorometer transects through packets, we have no data to assess the importance of this effect. However, the potential is clearly evident from the following estimates of light conditions at the chlorophyll maximum layer during internal wave packet passage.

With no internal wave packet active at Station A, the chlorophyll maximum layer was present at an average depth of about 10 m. The average Secchi depth of 10 m for the period of observations gives an approximate extinction coefficient of $k = 0.17\ m^{-1}$ (Poole and Atkins, 1929; Walker's [1980] revised relationship was not used). Therefore, the ambient light at the undisturbed chlorophyll maximum was approximately 18%. Using this same extinction coefficient when internal waves were present, and a depth variability of the chlorophyll maximum as great as 8 to 40 m due to internal waves, the greatest and least level at the chlorophyll maximum would be 26% and 0.1% of ambient surface illumination. This, of course, is the extreme condition. The fluctuations between these two levels occur on time scales of from 8 to 12 min. Since Kiefer (1973b) and Loftus and Seliger (1975) have shown that fluorescence of oceanic phytoplankton cells can vary as a function of irradiance on time scales as short as 2 min, fluorescence yields would be expected

to change in Massachusetts Bay as a function of the vertical and horizontal position of the phytoplankton in the internal wave packet. Within the depth range where photoinhibition of fluorescence occurs (Kiefer, 1973a), fluorescence yield changes should be observed in *in situ* fluorometer transects through internal wave packets.

In addition to making the interpretation of chlorophyll distribution patterns more difficult by affecting the fluorescence yield of plant cells, fluctuating light levels due to internal wave packets should also alter phytoplankton photosynthetic processes. Light levels experienced by cells in Massachusetts Bay vary on time scales of about (1) 12.4 hr for the semidiurnal internal tidal cycle, (2) 12 hr ± 3 (depending on season) for the day-night cycle, (3) a few hours for the modulations and natural variations of internal wave amplitudes within packets, and (4) 8-12 min for the period of the individual internal waves. The effects of these scales of fluctuation of light level on plant growth have been investigated by Kamykowski (*e.g.*, 1979) for the interaction of the day-night and 12.4 hr semidiurnal internal tidal cycles, by Marra (1978a,b) for light changes of one hour or more, by Savidge (1980) for changes of 5 to 45 min, and by Gallegos *et al.* (1980) for highly variable light regimes.

A simple model of the light level experienced by cells at the chlorophyll maximum layer over a period of 15 days serves to illustrate the longer-period (greater than an hour) variations that occur. The model used 11 m as the depth of the undisturbed chlorophyll maximum and an extinction coefficient of 0.17 m^{-1}. The temperature at the chlorophyll maximum was about 11°C. Light variations due to individual waves were ignored. The average depth of the chlorophyll maximum during packet passage was obtained by using the VCM 3 (Haury *et al.*, 1979, Fig. 3b) data for packet 5 (Fig. 2). The VCM followed the depth of the 10.5°C isotherm; thus it represented closely the depth history of a model phytoplankter in the chlorophyll maximum. The increase in depth of the 11°C isotherm at packet arrival to an average of 21 m was assumed to be instantaneous. The gradual decrease in average depth of the 11°C isotherm to the undisturbed depth of 11 m just prior to the arrival of the next packet 12.4 hr later was assumed to be linear. The daylight cycle of solar irradiance was assumed to be $I_t = I_o \sin\frac{\pi t}{12}$, with a light-dark cycle of 12h:12h and a maximum irradiance, I_o, just below the surface set at an arbitrary 100 light units. The model considered the plants to be passive, with no vertical migration in response to longer-term changes in light level.

Figure 20 shows the variation in incident radiation at the chlorophyll maximum over the 15-day period at Station A when packets like Packet 5 (Fig. 2) pass through the area. Of course, no single population of plant cells would experience this regime, since advection over the two-week period would carry them from the area. However, Figure 20 shows the light environment which phytoplankton would have to utilize at Station A under these conditions. Again using Packet 5 as an

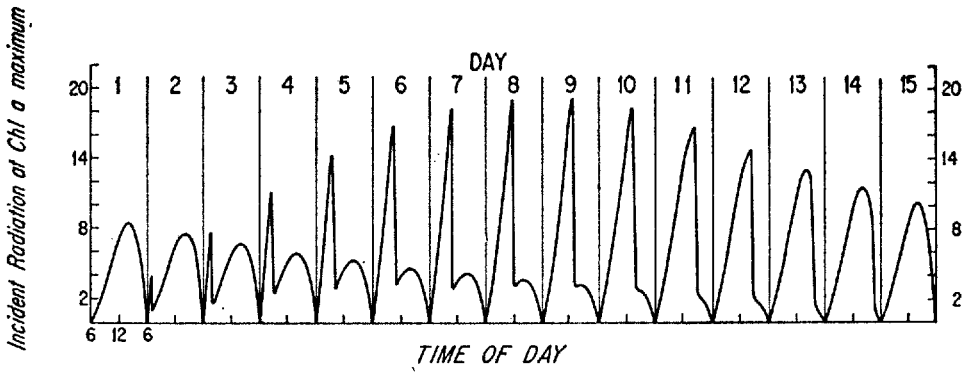

Figure 20. Daily variation in incident radiation at the chlorophyll maximum over a 15-day period at Station A. Maximum irradiance at noon arbitrarily set at 100 units. See text for details.

example, day-to-day peak irradiances due to internal wave effects alone differed by factors as large as 2.3. Integrated daily irradiance varied by up to 63%. After packet arrival, the light level would have varied with a period of about 10 min by factors of 16 for the first 4 hr, by 2.3 for the next 6 hr, and by 1.7 for the last 3 hr before arrival of the next packet. For more intense packets, short-period fluctuations of light could change by a factor of greater than 200. Given the implications of the studies of Marra (1978a,b), Kamykowski (1979), Gallegos *et al.* (1980), Savidge (1980), and the references cited therein, productivity estimates for Massachusetts Bay and other areas with internal waves of amplitudes large enough to significantly alter light levels must consider these effects.

It has been known for some time that internal waves and tides displace thermoclines and the associated nutriclines (*e.g.*, Armstrong and LaFond, 1966; Kelley, 1975). Direct evidence for the breaking of higher-frequency waves in oceanic thermoclines is sparse (*e.g.*, Woods and Wiley, 1972; Eriksen, 1978); such events are often only implied (*e.g.*, Krauss *et al.*, 1973; Dillon and Caldwell, 1978). Farmer and Smith (1980), however, have documented breaking waves in Knight Inlet (a fresh-water layer over salt water). Breaking internal waves have been suggested as an important cause of mixing (Thorpe, 1978) and as a mechanism for pumping nutrients into the nutrient-depleted surface layers (McGowan and Hayward, 1978). The breaking of large internal waves in the deep water of Massachusetts Bay at Station A, as shown in Haury *et al.* (1979), suggests that this phenomenon would contribute to the input of nutrients in the surface mixed layer. We have neither the nutrient data nor sufficient information on the temporal and areal extent of the breaking events to estimate the importance of these events to the overall nutrient budget of Massachusetts Bay. Evidence for breaking waves, however, was seen in nearly every wave packet acoustically observed between Stellwagen Bank and the western

side of the Bay. The deep-water breaking events appear to be restricted to the first few crests of the wave packets. Such occurrences could depend, for example, on temporal and areal variations in stratification, the presence or absence of mixing caused by previous overturning events, and on variations in internal wave amplitude caused by tidal current variations over Stellwagen Bank. This character of the waves would contribute to spatial and temporal heterogeneity in primary production in the surface layers through the localized and quasi-random injection of nutrients.

Breaking occurs frequently when the wave packets approach shoal water (less than 60 m deep) on the western side of Massachusetts Bay. Orr (1982) presents acoustic evidence of the large vertical and horizontal extent of this part of wave packet history. Since turbulence has been observed from the surface to near the bottom, not only should nutrients be mixed upward from below shallow thermoclines, but also detritus and finer sediments at the bottom could be resuspended and mixed upward when turbulent velocities are sufficiently high. This latter process has been observed and suggested as being important in shoal waters off Southern California (Emery and Gunnerson, 1973). The bottom of the western side of the Bay at depths of less than 50 m ranges from silty sand to gravel and glacial debris (Schlee *et al.*, 1973); some of these areas would be susceptible to resuspension. The acoustic data (Orr, 1982) suggests that in water less than 30 m deep, internal wave-caused mixing is near the thermocline. Turbulent flow toward deeper water occurs near the bottom, possibly due to mechanisms similar to those postulated by Emery and Gunnerson (1973) and studied by Stigebrandt (1976, 1979) for fjords. Once mixing by internal wave breaking occurred in shallow water, advection by the mean and tidal currents would carry the near-surface mixed water generally south and southeastward, potentially enhancing the primary production in this area. The deeper bottom flows, however, could carry some of the mixed water into the deeper water of the Bay, thus reducing the potential for enhanced primary production.

Acknowledgments. The help of many people was essential to the success of the experiment, the analysis of the data, and the preparation of the manuscript. In particular we thank the officers and crew of R/V *Oceanus*; B. Bardsley, S. Boyd, J. Brooks, T. Chereskin, T. Crook, J. Dean, A. Gargett, and E. Hays also participated in the cruise. S. Hoercher analyzed the plankton recorder samples. R. Ebey typed the many drafts of the manuscript. The graphics departments of the Woods Hole Oceanographic Institution and the Marine Life Research Group, Scripps Institution of Oceanography, prepared the figures. We also acknowledge the participation during the field observations of G. Garosi and L. Goodman, Naval Underwater Systems Center, Newport, Rhode Island, who were on board LCU 1647 with D. Crowell and J. Doutt from M. Orr's acoustic group; this cooperation was of particular assistance by giving us a two-ship view of the internal wave fields. F. Hess designed and supervised construction of the acoustic system. This material is based on research supported by the National Science Foundation under Grant No. OCE77-08682. Additional support was provided by the Marine Life Research Group of the Scripps Institution of Oceanography. Contribution No. 5132 from Woods Hole Oceanographic Institution.

REFERENCES

Angel, M. V. 1976. Windows into a sea of confusion: sampling limitations to the measurement of ecological parameters in oceanic mid-water environments, *in* Oceanic Sound Scattering Prediction, N. R. Anderson and B. J. Zahuranec, eds., Plenum, New York, 217–248.

Apel, J. R., H. M. Byrne, J. R. Proni and R. Sellers. 1976. A study of oceanic internal waves using satellite imagery and ship data. Remote Sensing of Environment, *5*, 125–135.

Apel, J. R., J. R. Holbrook and J. Tsai. 1980. The Sulu Sea internal soliton experiment. Part A: background and overview. (Abstract #0220) EOS, *61*, 1009.

Armstrong, F. A. J. and E. C. LaFond. 1966. Chemical nutrient concentrations and the relationship to internal waves and turbidity off Southern California. Limnol. Oceanogr., *11*, 538–547.

Bigelow, H. B. 1927. Physical oceanography of the Gulf of Maine. Bull. U.S. Bur. Fish., *40*, 511–1027.

Blackman, R. B. and J. W. Tukey. 1959. The Measurement of Power Spectra. Dover, New York, 190 pp.

Brown, N. L. 1974. A precision CTD microprofiler. Proc. Int. Congress Engineering Ocean Environ., Halifax, Nova Scotia, *2*, 270–278.

Carsola, A. J. and E. B. Callaway. 1962. Two short-period internal wave frequency spectra in the sea off Southern California. Limnol. Oceanogr., *7*, 115–120.

Curtin, T. B. and C. N. K. Mooers. 1975. Observation and interpretation of a high-frequency internal wave packet and surface slick pattern. J. Geophys. Res., *80*, 882–894.

Denman, K. L. 1976. Covariability of chlorophyll and temperature in the sea. Deep-Sea Res., *23*, 539–550.

Derenbach, J. B., H. Astheimer, H. P. Hansen and H. Leach. 1979. Vertical microscale distribution of phytoplankton in relation to the thermocline. Mar. Ecol. Prog. Ser., *1*, 187–193.

Dillon, T. M. and D. R. Caldwell. 1978. Catastrophic events in a surface mixed layer. Nature, *276*, 601–602.

Emery, K. O. and C. G. Gunnerson. 1973. Internal swash and surf. Proc. Nat. Acad. Sci. U.S.A., *70*, 2379–2380.

Eriksen, C. C. 1978. Measurements and models of fine structure, internal gravity waves, and wave breaking in the deep ocean. J. Geophys. Res., *83*, 2989–3009.

Ewing, G. 1950. Slicks, surface films and internal waves. J. Mar. Res., *9*, 161–187.

Farmer, D. M. and J. D. Smith. 1980. Tidal interaction of stratified flow with a sill in Knight Inlet. Deep-Sea Res., *27*, 239–254.

Fisher, R. A. 1958. Statistical Methods for Research Workers. Hafner Publ., New York, 356 pp.

Gallegos, C. L., G. M. Hornberger and M. G. Kelley. 1980. Photosynthesis-light relationships of a mixed culture of phytoplankton in fluctuating light. Limnol. Oceanogr., *25*, 1082–1092.

Gargett, A. E. and B. A. Hughes. 1972. On the interaction of surface and internal waves. J. Fluid Mech., *52*, 179–191.

Gregg, M. C. and M. G. Briscoe. 1979. Internal waves, finestructure, microstructure, and mixing in the ocean. Rev. Geophys. Space Phys., *17*, 1524–1548.

Halpern, D. 1971. Observations on short-period internal waves in Massachusetts Bay. J. Mar. Res., *29*, 116–132.

Haury, L. R. 1976. Small-scale pattern of a California Current zooplankton assemblage. Mar. Biol., *37*, 137–157.

Haury, L. R., M. G. Briscoe and M. H. Orr. 1979. Tidally generated internal wave packets in Massachusetts Bay. Nature, *278*, 312–317.

Haury, L. R., J. A. McGowan and P. H. Wiebe. 1978. Patterns and processes in the time-space scales of plankton distributions, *in* Spatial Pattern in Plankton Communities, J. H. Steele, ed., Plenum, New York, 277–327.

Haury, L. R., P. H. Wiebe and S. H. Boyd. 1976. Longhurst-Hardy Plankton Recorders: their design and use to minimize bias. Deep-Sea Res., *23*, 1217–1229.

Holbrook, J. R., J. R. Apel and J. Tsai. 1980. The Sulu Sea internal soliton experiment. Part B: Observations of large-amplitude, nonlinear internal waves. (Abstract #0221) EOS, *61*, 1009.

Hunt, M. 1977. A program for spectral analysis of time series. Tech. Memo. No. 2-77, Woods Hole Oceanographic Institution, 188 pp.

Joyce, T., J. Dean, M. McCartney, R. Millard, D. Moller, A. Voorhis, C. Dahm, D. Georgi, G. Kullenberg, J. Toole, and W. Zenk. 1976. Observations of the Antarctic Polar Front during FDRAKE 76: A cruise report. Woods Hole Oceanographic Institution Tech. Rep. 76-74, 150 pp.

Kamykowski, D. L. 1972. Some physical and chemical aspects of the phytoplankton ecology of La Jolla Bay. Ph.D. thesis, Univ. Calif. San Diego, 269 pp.

—— 1974. Possible interactions between phytoplankton and semidiurnal internal tides. J. Mar. Res., *32*, 67–89.

—— 1976. Possible interactions between plankton and semidiurnal internal tides: II. Deep thermocline and trophic effects. J. Mar. Res., *34*, 499–509.

—— 1979. The growth response of a model *Gymnodinium splendens* in stationary and wavy water columns. Mar. Biol., *50*, 289–303.

Kelley, J. C. 1975. Time-varying distributions of biologically significant variables in the ocean. Deep-Sea Res., *22*, 679–688.

—— 1976. Sampling the sea, *in* The Ecology of the Seas, D. H. Cushing and J. J. Walsh, eds., Saunders, Phila., 361–387.

Kiefer, D. A. 1973a. Fluorescence properties of natural phytoplankton populations. Mar. Biol., *22*, 263–269.

—— 1973b. Chlorophyll *a* fluorescence in marine centric diatoms: responses of chloroplasts to light and nutrient stress. Mar. Biol., *23*, 39–46.

Krauss, W., P. Koske and J. Kielmann. 1973. Observations on scattering layers and thermoclines in the Baltic Sea. Kiel. Meeresforsch., *29*, 85–89.

LaFond, E. C. and K. G. LaFond. 1972. Sea surface features. J. Mar. Biol. Assoc. India, *14*, 1–14.

Loftus, M. E. and H. H. Seliger. 1975. Some limitations of the *in vivo* fluorescence technique. Chesapeake Sci., *16*, 79–92.

McGowan, J. A. and T. L. Hayward. 1978. Mixing and oceanic productivity. Deep-Sea Res., *25*, 771–793.

Marra, J. 1978a. Effect of short-term variations in light intensity on photosynthesis of a marine phytoplankter: a laboratory simulation study. Mar. Biol., *46*, 191–202.

—— 1978b. Phytoplankton photosynthetic response to vertical movement in a mixed layer. Mar. Biol., *46*, 203–208.

Maxworthy, T. 1979. A note on the internal waves produced by tidal flow over a three-dimensional ridge. J. Geophys. Res., *84*, 338–346.

Orr, M. H. 1981. Remote acoustic detection of zooplankton response to fluid processes, oceanographic instrumentation, and predators. Can. J. Fish. Aquatic Sci., *38*, 1096–1105.

—— 1982. Short-period internal waves in Massachusetts Bay: development, decay and associated mixing processes. J. Mar. Res., (submitted).

Orr, M. H. and F. R. Hess. 1978. Remote acoustic monitoring of natural suspensate distributions, active suspensate resuspension, and slope/shelf water intrusions. J. Geophys. Res., *83*, 4062–4068.

Osborne, A. R. and T. L. Burch. 1980. Internal solitons in the Andaman Sea. Science, *208*, 451–460.

Otnes, R. K. and L. Enochson. 1978. Applied Time Series Analysis. Vol. 1, Basic Techniques. Wiley, New York, 449 pp.

Poole, H. H. and W. R. G. Atkins. 1929. Photo-electric measurements of sub-marine illumination throughout the year. J. Mar. Biol. Assoc. U.K., *16*, 297–324.

Savidge, G. 1980. Photosynthesis of marine phytoplankton in fluctuating light regimes. Mar. Biol. Lett., *1*, 295–300.

Sawyer, C. and J. R. Apel. 1976. Satellite images of ocean internal-wave signatures. U.S. Dept. Comm., Nat. Oceanic Atmos. Admin., Environ. Res. Lab., NOAA S/T 2401, 17 sheets.

Schlee, J. D., D. W. Folger and C. J. O'Hara. 1973. Bottom sediments on the continental shelf off the northeastern United States—Cape Cod to Cape Ann, Massachusetts. U.S. Geol. Surv., Misc. Geol. Invest., Map I-746.

Stigebrandt, A. 1976. Vertical diffusion driven by internal waves in a sill fjord. J. Phys. Oceanogr., *6*, 486–495.

—— 1979. Observational evidence for vertical diffusion driven by internal waves of tidal origin in the Oslo fjord. J. Phys. Oceanogr., *9*, 435–441.

Tate, M. W. and R. C. Clelland. 1957. Nonparametric and Shortcut Statistics. Interstate, Danville, Ill., 171 pp.

Thorpe, S. A. 1978. The near-surface ocean mixing layer in stable heating conditions. J. Geophys. Res., *83*, 2875–2885.

Voorhis, A. D. 1968. Measurements of vertical motion and the partition of energy in the New England slope water. Deep-Sea Res., *15*, 599–608.

Walker, T. A. 1980. A correction to the Poole and Atkins Secchi disc/light-attenuation formula. J. Mar. Biol. Assoc. U.K., *60*, 769–771.

Woods, J. D. and R. L. Wiley. 1972. Billow turbulence and ocean microstructure. Deep-Sea Res., *19*, 87–121.

Wyatt, T. 1975. The limitations of physical models for red tides, *in* First Int. Conf. Toxic Dinoflagellate Blooms, V. R. LoCicero, ed., Mass. Sci. and Technol. Found., Waterfield, Mass., 81–93.

Received: *2 July, 1982*; revised: *28 September, 1982.*